JBC RESEARCH ARTICLE

Effect of clinical isolate or cleavage site mutations in the SARS-CoV-2 spike protein on protein stability, cleavage, and cell–cell fusion

Received for publication, January 22, 2021, and in revised form, June 8, 2021 Published, Papers in Press, June 20, 2021,
https://doi.org/10.1016/j.jbc.2021.100902

Chelsea T. Barrett[1], Hadley E. Neal[1], Kearstin Edmonds[1], Carole L. Moncman[1], Rachel Thompson[1], Jean M. Branttie[1], Kerri Beth Boggs[1], Cheng-Yu Wu[1], Daisy W. Leung[2], and Rebecca E. Dutch[1,*]

From the [1]Department of Molecular and Cellular Biochemistry, University of Kentucky, Lexington, Kentucky, USA; [2]Division of Infectious Diseases, Department of Medicine, Washington University School of Medicine in St Louis, St Louis, Missouri, USA

Edited by Craig Cameron

The trimeric severe acute respiratory syndrome coronavirus 2 (SARS-CoV-2) spike protein (S) is the sole viral protein responsible for both viral binding to a host cell and the membrane fusion event needed for cell entry. In addition to facilitating fusion needed for viral entry, S can also drive cell–cell fusion, a pathogenic effect observed in the lungs of SARS-CoV-2–infected patients. While several studies have investigated S requirements involved in viral particle entry, examination of S stability and factors involved in S cell–cell fusion remain limited. A furin cleavage site at the border between the S1 and S2 subunits (S1/S2) has been identified, along with putative cathepsin L and transmembrane serine protease 2 cleavage sites within S2. We demonstrate that S must be processed at the S1/S2 border in order to mediate cell–cell fusion and that mutations at potential cleavage sites within the S2 subunit alter S processing at the S1/S2 border, thus preventing cell–cell fusion. We also identify residues within the internal fusion peptide and the cytoplasmic tail that modulate S-mediated cell–cell fusion. In addition, we examined S stability and protein cleavage kinetics in a variety of mammalian cell lines, including a bat cell line related to the likely reservoir species for SARS-CoV-2, and provide evidence that proteolytic processing alters the stability of the S trimer. This work therefore offers insight into S stability, proteolytic processing, and factors that mediate S cell–cell fusion, all of which help give a more comprehensive understanding of this high-profile therapeutic target.

Severe acute respiratory syndrome coronavirus 2 (SARS-CoV-2) is the causative viral agent of the ongoing coronavirus disease 2019 (COVID-19) global pandemic. Thus far, COVID-19 has impacted over 86 million people globally, resulting in the death of more than one and a half million individuals (https://covid19.who.int/). Because of the widespread global impact of this pandemic, a concerted effort has been made to rapidly develop a vaccine or an antiviral treatment.

The SARS-CoV-2 spike (S) protein is the major transmembrane glycoprotein studding the surface of the viral particle and is exclusively responsible for viral attachment and cell entry, thus making it the major target of current vaccine strategies and antiviral therapeutics (1). The S protein consists of two distinct subunits: the S1 subunit, which binds to the known host receptor, angiotensin-converting enzyme 2 (ACE2) (2–10), and the S2 subunit that promotes the viral-to-host cell membrane fusion event needed for viral infection (1, 7, 11–17). Most known coronavirus (CoV) S proteins undergo two post-translational proteolytic cleavage events, one at the border of the S1 and S2 subunits and one downstream within the S2 subunit (termed S2') (1, 12, 14–20).

Similar to several other CoVs, SARS-CoV-2 likely utilizes bats as a reservoir species, specifically *Rhinolophus affinis* or horseshoe bats (10, 21–24). SARS-CoV-2 has 96% sequence identity to a CoV found in this bat population, RaTG13, with limited differences between them (24). One difference is the polybasic, PRRA, insertion at the S1/S2 border, which gives this site the canonical sequence requirements for cleavage by the cellular proprotein convertase furin (25–28). This change may be a key factor in the zoonotic transmission of SARS-CoV-2. The presence of a furin consensus sequence at the cleavage site has been observed in other human-infecting CoVs (25, 29–31) as well as in highly pathogenic forms of influenza (32, 33), and previous studies have demonstrated its functional significance. For SARS-CoV-2, the insertion is suggested to allow for expanded cellular tropism and infectivity (12, 25, 34, 35). For most CoVs, cleavage at a downstream S2' site may be carried out by a number of cellular proteases, including serine proteases like transmembrane serine protease 2 (TMPRSS2), or endopeptidases, including members of the cathepsin family (12, 13, 18–20).

Following receptor binding by the S1 subunit and priming by proteolytic cleavage, the S2 subunit of S promotes the critical membrane fusion step of viral entry by undergoing dynamic conformational changes to promote merging of the viral and host cell membranes (9, 34, 36). For entry of SARS-CoV-2, cleavage at the S1/S2 border (by furin or a similar protease) is critical for TMPRSS2 cleavage and entry at the plasma membrane. However, when S1/S2 border cleavage is blocked, viral entry can be mediated through endosomal compartments with proteolytic cleavage carried out by a member of the cathepsin family, similar to the entry pathway

* For correspondence: Rebecca E. Dutch, rdutc2@uky.edu.

of SARS-CoV (9, 34, 36–38). In addition to promoting virus–cell fusion during viral particle entry, S can also promote cell–cell fusion, a pathogenic effect observed in the lungs of patients with COVID-19 where neighboring cells fuse together to form large multinucleated cells, termed syncytia (39–44). While the role of cellular proteases and S cleavage in viral entry is being extensively investigated, insight into the cleavage requirements for cell–cell fusion in SARS-CoV-2 remains more limited. Recent studies have suggested that S cleavage at the S1/S2 border is critical for cell–cell fusion, and TMPRSS2, while not required, appears to enhance this cell–cell fusion (36, 39, 45, 46). However, relatively little is known about the timing and efficiency of these cleavage events, and how mutations in S may affect the process.

Though CoVs mutate at a slower rate than most RNA viruses because of the presence of viral proofreading machinery, a meta-analysis of genomes of circulating SARS-CoV-2 found several mutations within S circulating in significant percentages of the analyzed populations (47, 48). The most common mutation, now found in most of the global population, is an aspartate to glycine mutation at residue 614 (D614G) in the S1 subunit. Additional mutations throughout the S1 and S2 subunits of S have been found in a smaller percentage of the viral population. Since S2 contains the fusion machinery, mutations in this region may have an impact on overall protein stability and fusion. Understanding the effects of mutations in this region will allow for a more comprehensive understanding of the overall S function.

We tested WT SARS-CoV-2 S and variants in different host cell lines to analyze the effects on stability, proteolytic processing, and cell–cell fusion. Here, we demonstrate that furin cleavage of S at the S1/S2 border is required for efficient cell–cell fusion and that the presence of TMPRSS2 in target cells enhances S-mediated cell–cell fusion, consistent with previous studies (36, 45). We also show that mutations of the cleavage sites at the S1/S2 border, S2' site, or a cathepsin L (cath L) cleavage site, conserved from SARS-CoV S, all reduce initial cleavage at the S1/S2 border during viral protein synthesis, suggesting that mutations downstream of the S1/S2 border likely alter the overall conformation of the protein. In addition, we identify two S2 subunit residues, one in the internal fusion peptide and another in the cytoplasmic tail, which alter protein fusion function when mutated without changing overall protein expression and cleavage, providing more insight into regions of the protein important for the regulation of the fusion process. Finally, we demonstrate protein turnover and cleavage kinetics in a range of host cells as well as in the presence of several exogenous proteases, providing a more comprehensive picture of the S protein.

Results

Stability and proteolytic cleavage of SARS-CoV-2 spike in relevant cell lines

To examine the stability and cleavage patterns of SARS-CoV-2 S in a range of mammalian cell lines, several cell lines were transiently transfected with pCAGGS-S. We used Vero cells, an easily transfectable cell line frequently used in the field, A549 cells, a human adenocarcinoma alveolar basal epithelial cell line, to better understand S in a more relevant cell model, cath L-mouse embryonic fibroblast (MEF), a previously generated cath L knockout cell line used to understand the contribution of cath L to S processing, WT MEFs, as a control to the cath L-line, and LoVo cells, a human colon carcinoma line that does not express functional furin to allow for analysis of the role of furin. Stability of S and the timing of proteolytic processing were determined by pulse-chase labeling and immunoprecipitation. S protein detected from immunoprecipitation with an S2 subunit–specific antibody was observed as two bands, a band around 150 kDa corresponding to an uncleaved full-length species of the protein, labeled S, and a band around 97 kDa corresponding to a species of S cleaved at the border of the S1 and S2 subunits, labeled S2 (Fig. 1*A*; reference gel with molecular weight markers and expected band positions for S2 and the S2' [not visualized] in Fig. S1*E*). After a 1-h chase, a band corresponding to S2 was observed in Vero, A549, and both MEF cell lines (Fig. 1*A*). In LoVo cells, a band corresponding to the S2 subunit did not appear until 4 h of chase, verifying that lack of furin impedes efficient processing at S1/S2, and that the S1/S2 border can be cleaved by cellular protease other than furin (Fig. 1*A*) in a slower and less efficient process. Vero cells, A549 cells, MEFs, and cath L-MEFs displayed similar cleavage patterns over time, whereas LoVo cells displayed significantly less cleavage at 2 and 4 h. LoVo cells had only 2% cleavage at 2 h and 18% cleavage at 4 h, compared with about 20 to 40% at 2 h and 30 to 60% at 4 h for all other cell types ($p < 0.05$). However, LoVo cells reached cleavage levels similar to the other cell lines at later chase time points (Fig. 1*B*). Bands smaller than 90 kDa that would correspond to cleavage at the S2' site were not observed in any cell line (the expected position of this band is noted on the full-length gel in Fig. S1*E*). In the examined cell lines, expressed S remained stable through the first 4 h (Fig. 1*C*). By 24 h after label, only 20 to 30% of the original labeled protein remained for all cell lines.

Several studies have examined the cellular proteases involved in the cleavage of S. Furin and TMPRSS2 appear to play key roles in cleavage at the S1/S2 border and S2' site, respectively (9, 25, 34, 49, 50). In addition, lysosomal proteases such as cath L/B can be utilized for viral entry in TMPRSS2-deficient cells (9, 37, 45). To examine how higher expression levels of these proteases affect S stability and cleavage, Vero and A549 cells were transiently transfected with S alone or S with TMPRSS2, furin, or cath L. Pulse-chase analysis demonstrated that the transient expression of TMPRSS2 or cath L did not affect the cleavage pattern of S (Fig. 1, *D* and *E* and Fig. S1*B*), and a band corresponding to S2' cleavage was not observed in either Vero or A549 cells. However, transient overexpression of furin increased the cleavage observed at the S1/S2 border in Vero cells at 4 and 8 h of chase ($p < 0.05$) and at all times after zero for A549 cells ($p < 0.01$ for 1- and 8-h chase, $p < 0.0001$ for 2-

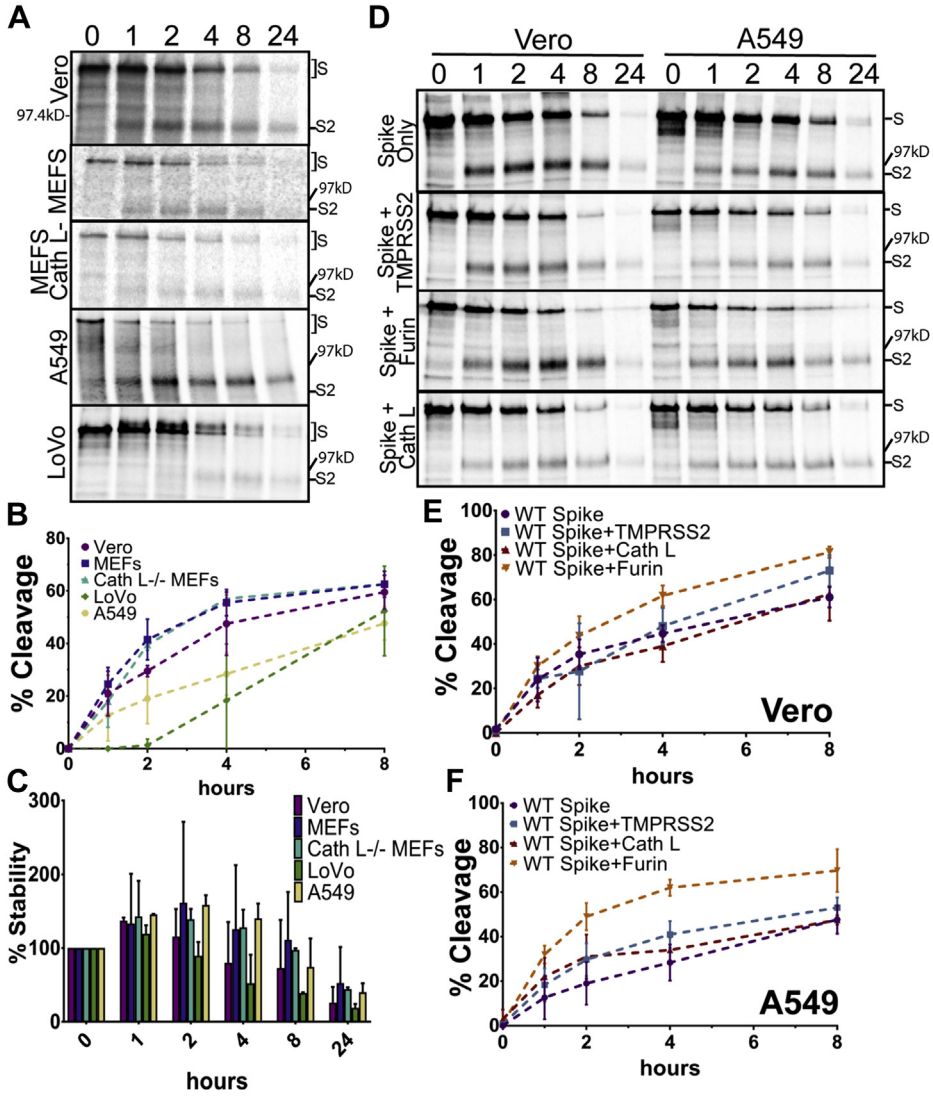

Figure 1. SARS-CoV-2 spike is cleaved at the S1/S2 subunit border in a variety of cell lines. *A*, the indicated cell types transiently expressing S were metabolically labeled for 1 h and chased for times indicated (hours). Band densitometry was used to quantify bands representing full-length S or S cleaved at the S1/S2 border (S2). *B*, percent cleavage (S2 divided by S plus S2) and (*C*) overall protein stability (total S, S plus S2, for each time point, normalized to time point 0) were calculated for spike in each cell line (n = 3). *D*, Vero cells or A549 cells transiently expressing S alone or S with proteases were metabolically labeled and chased for the times indicated (hours). Percent cleavage was measured using band densitometry in both (*E*) Vero and (*F*) A549 cells (*B*, *C*, *E*, and *F* are represented as the average ± SD for three independent experiments). S, spike protein; SARS-CoV-2, severe acute respiratory syndrome coronavirus 2.

and 4-h chase times) (Fig. 1, *E* and *F*). This suggests that the normal levels of cellular furin can eventually promote maximal levels of S1/S2 cleavage in both Vero and A549 cells, but overexpression of furin facilitates more rapid cleavage of the S1/S2 border. Interestingly, in both experiments (Fig. 1, *A* and *D*), some uncleaved S remains even after 24 h, indicating that a small portion of the S population is not cleaved by furin or other endogenous proteases in these cell lines. Overall protein stability was not affected by coexpression of any tested proteases (Fig. S1*B*). Finally, to further analyze the capability of each of these proteases to cleave the S protein, we transiently transfected S with furin, TMPRSS2, or cath L in LoVo cells since they demonstrated a significant reduction in S protein cleavage compared with other cell lines tested. Only coexpression with furin appeared to restore S protein cleavage at the S1/S2 border (Fig. S2*E*).

Spike-mediated cell–cell fusion

The S2 subunit of S mediates both viral–cell fusion and cell–cell fusion (39–41), with cell–cell fusion readily observed both in a laboratory setting and in the lungs of SARS-CoV-2–infected patients (39–44). To better understand the requirements and contribution of cellular proteases to S2-mediated cell–cell fusion, we performed syncytia and reporter gene assays. For syncytia analysis, a small number of syncytia were observed at 24 h post transfection (hpt) in all samples (Fig. 2*A*). At 48 hpt, similar numbers of large syncytia were observed with S alone or S coexpressed with TMPRSS2

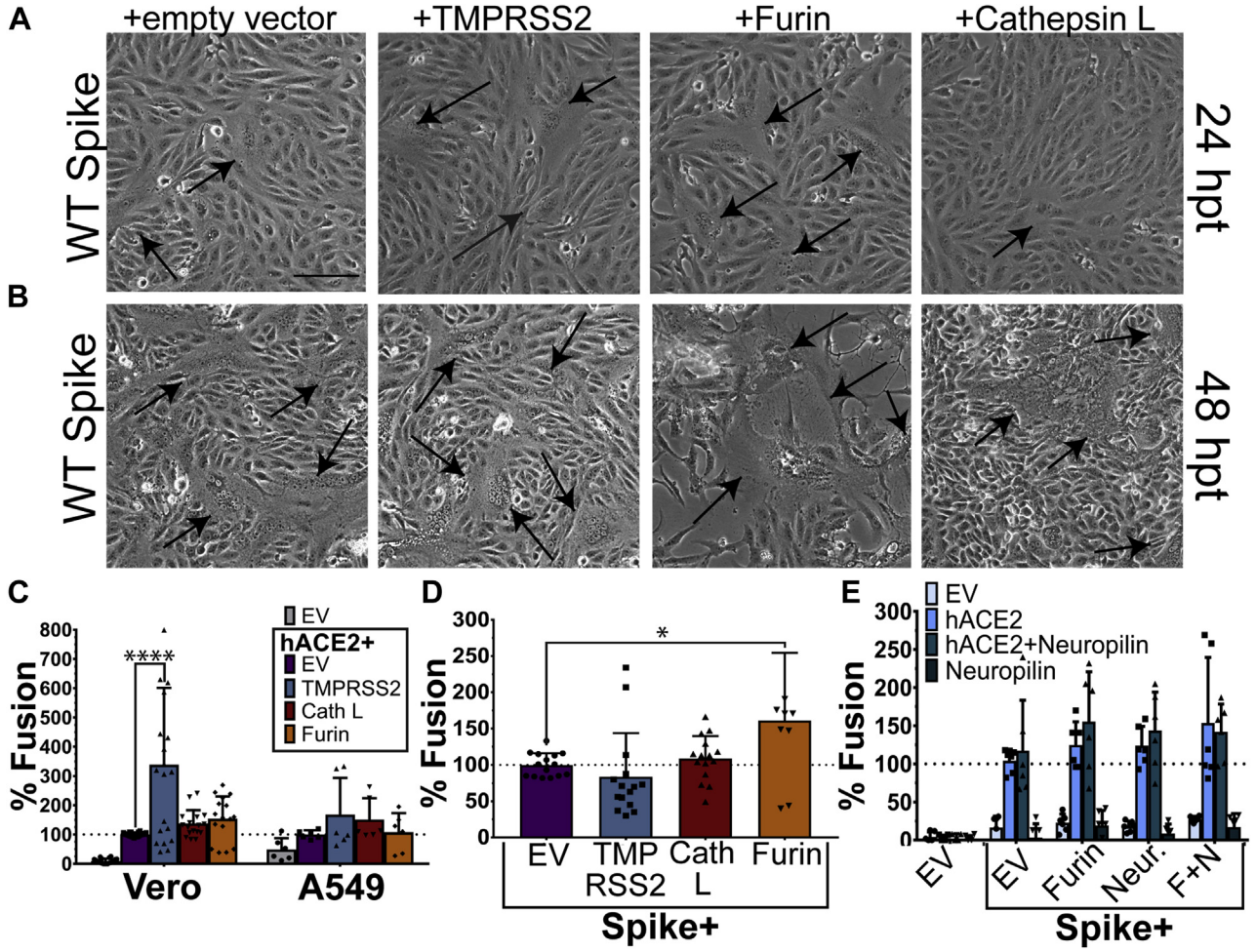

Figure 2. CoV-2 spike alone mediates cell–cell fusion. Vero cells expressing S and TMPRSS2, furin, or cathepsin L were imaged at 24 (*A*) and 48 (*B*) hpt for syncytia formation (*black arrows*). Magnification bar is 100 μM. *C*, a luciferase reporter gene assay was performed with target cells (BSR/T7 cells expressing hACE2 and additional proteases) overlaid onto effector cells (Vero or A549 cells expressing S) for 9 h. *D*, luciferase reporter gene experiment was performed with additional proteases coexpressed with S in Vero cells and overlaid with target cells expressing hACE2. *E*, the effect of neuropilin in both target and effector (Vero) cells was examined with a luciferase reporter gene assay. Expression of effector cells is listed along the *x*-axis. Target cell expression is listed in the legend to the graph. Results expressed as the percent fusion normalized to samples with S in the effector cells and hACE2 only in the target cells (*C–E* are average ± SD for three independent experiments, performed in duplicate). Significance was determined by two-way ANOVA. $*p < 0.05$, $****p < 0.0001$. CoV-2, coronavirus 2; hACE2, human angiotensin-converting enzyme 2; hpt, hours post transfection; S, spike protein; TMPRSS2, transmembrane serine protease 2.

or cath L (Fig. 2*B*). However, coexpression of S with furin resulted in increased syncytia formation. The cells exhibited nearly complete fusion, suggesting that the presence of exogenous furin further increases S-mediated cell–cell fusion (Fig. 2*B*, *panel 3*).

To quantitate S-mediated cell–cell fusion, luciferase reporter gene fusion assays were performed (Fig. S2*A*), using a 9-h overlay that was determined to be optimal (Fig. S2*B*). To characterize the role of cellular proteases in the human ACE2 (hACE2)–expressing target cells, S-expressing effector cells were overlaid with target cells containing hACE2 alone or hACE2 with TMPRSS2, furin, or cath L. The amount of plasmid transfected was kept constant by supplementing with a plasmid encoding an empty expression vector (EV). When Vero cells were used as the S-expressing effector cell and TMPRSS2 was present in the target cells, a significant increase in fusion was observed. This is consistent with the concept that TMPRSS2 plays a role in fusion after or during the hACE2 (receptor)-binding step in the fusion cascade (Fig. 2*C*) (9, 11, 31, 36, 45), although the presence of TMPRSS2 in these target cells also appeared to process hACE2 (Fig. S2*C*, also observed in Ref. (39)). In samples with cath L or furin in the target cells, fusion levels were similar to hACE2 + EV (Fig. 2*C*). When A549 cells were used as the S-expressing effector cell, none of the conditions produced statistically significant differences from background levels (Fig. 2*C*), so Vero cells were used as the effector cells for the remainder of the experiments performed.

Having analyzed the function of proteases in the target cells, we were also interested in the role of proteases present in the S-expressing effector cells. To test this, EV, TMPRSS2, cath L, or furin was coexpressed with S, and samples were overlaid with target cells expressing hACE2 (Fig. 2*D*). Similar to what we observed in syncytia assays, only coexpression of S and furin produced a statistically significant increase in fusion (Fig. 2*D*). This increase is likely because of the increase in the

amount of cleaved protein present when S is coexpressed with furin (Fig. 1*E*).

Neuropilin-1 has been suggested as a coreceptor for SARS-CoV-2 S and may be important for the viral infection infiltrating the neuronal network (51–53). To assess the contribution of neuropilin in cell–cell fusion, effector cells were transfected with S and either EV, furin, neuropilin, or furin and neuropilin (F + N). Target cells were transfected with EV, hACE2, neuropilin, or hACE2 and neuropilin (neuropilin expression verified by Western blot, shown in Fig. S2*D*). However, no significant increase in fusion was observed when neuropilin was present in either the target or effector cells (Fig. 2*E*), suggesting that neuropilin does not appear to play a significant role in cell–cell–mediated fusion. Interestingly, when neuropilin is coexpressed in S-containing effector cells, there is no difference observed in fusion compared with samples with S + EV, suggesting that neuropilin also does not have an inhibitory effect (Fig. 2*E*). In addition, when neuropilin alone is expressed in the target cells, fusion levels above background levels are not observed. This indicates that in cell–cell fusion, S-binding hACE2 appears to be the major interaction during the receptor attachment function.

Importance of CoV-2 cleavage sites

Early protein sequence analysis of CoV-2 S protein demonstrated the presence of three potential cleavage sites (25): a putative furin cleavage site at the S1/S2 border; a conserved site 10 residues downstream from the S1/S2 border, shown to be cleaved by cath L in SARS-CoV; and the S2' site that is potentially cleaved by TMPRSS2 (25). To functionally understand the role of each cleavage site in S cell–cell fusion, a series of mutants were made. Alanine mutations of all the residues within each potential cleavage site (S1/S2 AAAAA, cath L AAAA, and S2' AA) and single alanine mutations at the terminal arginine of the S1/S2 border and S2' site (S1/S2 PRRAA, S2' KA) were created. Finally, a mutant with residues (PRRA) upstream of the S1/S2 border deleted (del. PRRA), leaving a single R residue at this site, was made, creating an S1/S2 border similar to SARS-CoV S (Fig. 3*A*). Pulse-chase analysis (Fig. 3*B*) showed that all mutants exhibited similar protein degradation compared with WT S in Vero cells. However, in A549s, several mutants demonstrated more rapid protein turnover than WT S at later chase time points. Surprisingly, mutations at all three sites led to either a complete loss or a significant delay in the proteolytic processing of the S protein at the S1/S2 border, indicated by the lack of a band corresponding to the S2 subunit. This suggests that mutations at distal sites can strongly influence cleavage at S1/S2. After an 8-h chase, no cleavage at the S1/S2 border was observed for the mutants del. PRRA and S1/S2 AAAAA, confirming that deletion or mutation of the furin consensus prevents cleavage at this site. For all other mutants, cleavage at the S1/S2 border reached 30 to 50% of WT levels in both Vero and A549 cells at the 8-h time point (Fig. 3, *C* and *D*). Accurate analysis of protein cleavage was not possible by the 24-h time point since only 20 to 30% of protein remained (Fig. S1*B*). Finally, surface biotinylation showed that both total and cell surface expression of all mutants were not significantly different from WT S levels (Fig. 3, *E*–*G*). Similar to the results discussed previously, a band corresponding to cleavage at the cath L site or the S2' site was not observed in any condition tested.

To assess the effects of the mutations on cell–cell fusion, syncytia formation assays in Vero cells were performed. While syncytia were readily observed in all samples containing WT S, none of the mutants exhibited syncytia formation at 24 or 48 hpt when expressed alone (Fig. S3, *panel 2*). Addition of TMPRSS2 did not recover syncytia formation in any mutant (Fig. S3, *panel 3*), and the addition of furin only recovered syncytia formation in the S1/S2 PRRAA mutant (Fig. S3, *panel 4*, syncytia denoted with *black arrows*). To analyze this result, cells were lysed following the 48-h imaging, and protein levels were examined by Western blot. Results showed that coexpression of furin with the S1/S2 PRRAA mutant restored cleavage at the S1/S2 border, whereas all other mutants did not show cleavage at this site (data not shown). This suggests that cleavage at the S1/S2 border is critical for cell–cell fusion, and that the double R motif in the PRRAA mutant can be cleaved by overexpressed furin.

Luciferase reporter gene analysis of fusion in Vero cells transfected with WT S or each mutant showed similar results to the syncytia assays, with none of the mutants showing fusion levels above background (Fig. 3*H*). While the S2' AA mutant displayed fusion levels around 25%, these levels were not significantly above background levels. Reporter gene assays were also carried out with addition of transiently expressed furin in the S-expressing effector cells, but no significant increases in fusion were observed. Since all cleavage mutants created reduced cleavage at the S1/S2 subunit border, the reductions in cell–cell fusion may be attributable to loss of cleavage at this site.

Effect of circulating S mutations on protein stability, cleavage, and fusion

An early examination revealed several mutations in the S protein gene in circulating viral variants (47, 48), including the D614G substitution now found in most of the global SARS-CoV-2 (47, 54–60). The D614G mutation lies in the S1 subunit of the protein, just downstream of the receptor-binding domain and is proposed to play a critical role in receptor binding by alteration of the positioning of the receptor-binding domain. Other mutations in circulating variants were found throughout the S2 subunit (48). To assess the effect(s) of these mutations, we created the mutants D614G, A831V, D839Y/N/E, S943P, and P1263L (Fig. 4*A*). Pulse-chase analysis in Vero and A549 cells (Fig. 4*B*) demonstrated that all circulating mutants tested exhibited protein turnover (Fig. S1*D*) and protein cleavage (Fig. 4*C*) at similar rates as WT S in both cell lines. Surface biotinylation confirmed that all tested mutants displayed total protein and surface protein levels comparable to WT S, suggesting that none of the mutants caused major defects or enhancement of protein trafficking to the cell surface (Fig. 4,

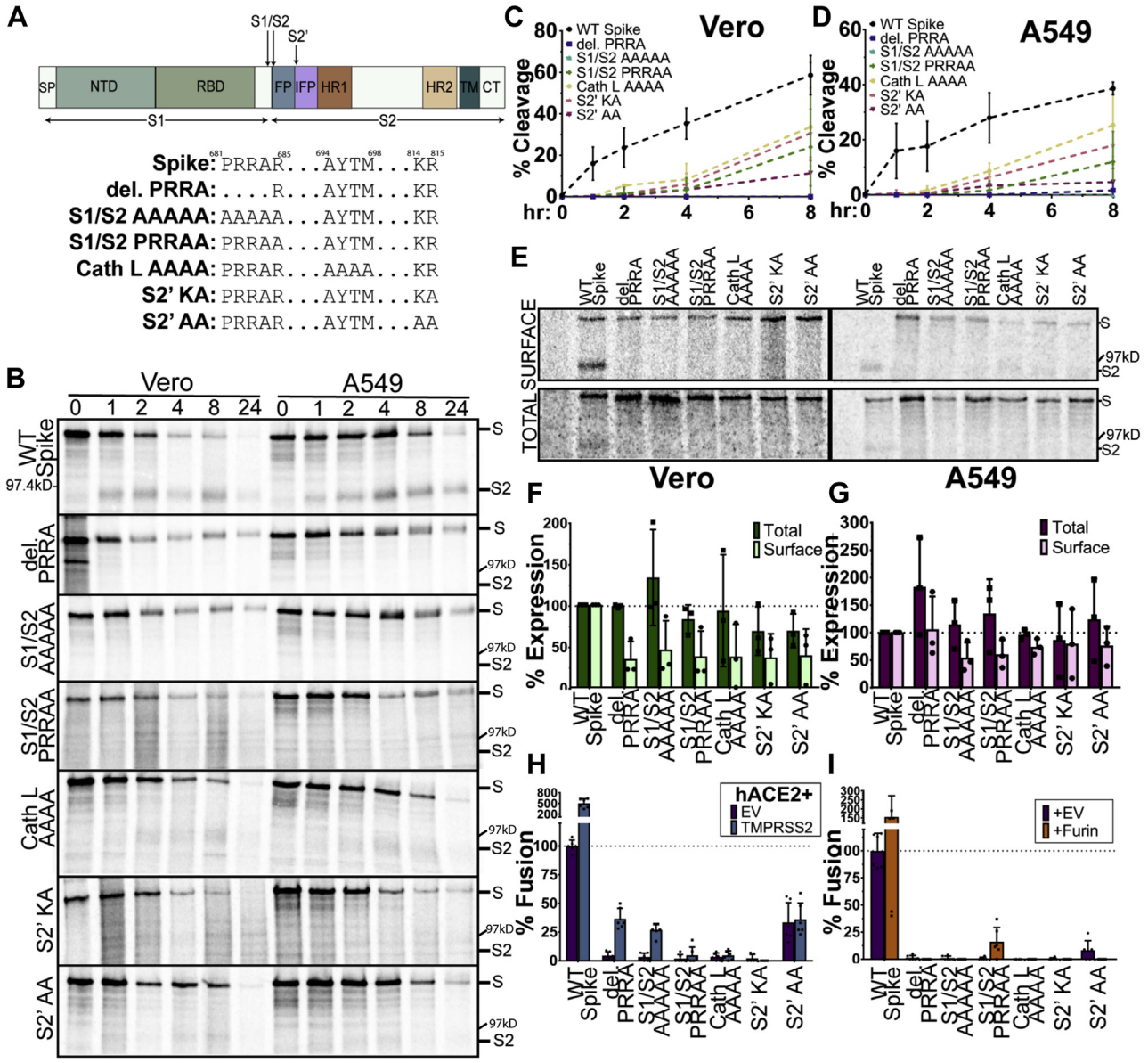

Figure 3. Mutations at all three potential spike cleavage sites reduce cleavage at the S1/S2 subunit border. *A*, full or partial alanine substitution mutations were made at each of the three potential cleavage sites. *B*, plasmids expressing WT S or mutants were transfected into Vero and A549 cells, cells were metabolically labeled for 1 h, and chased for the times indicated. Percent cleavage was determined in (*C*) Vero cells and (*D*) A549 cells (average ± SD for three independent experiments). *E*, surface biotinylation was performed on cells expressing WT S and each mutant. Cells were radiolabeled for 6 h. Protein expression in (*F*) Vero and (*G*) A549 cells, results are normalized to WT S, and error bars represent the SD (average ± SD for three independent experiments). *H*, a luciferase reporter gene assay was performed using target cells expressing hACE2 and EV or TMPRSS2, and effector (Vero) cells with WT S or each mutant. *I*, luciferase reporter gene analysis with cells expressing hACE2 and effector (Vero) cells transfected with S or S mutants and EV or furin-expressing plasmids. Results of both reporter gene assays are shown normalized to samples with WT S in the effector with hACE2 in target cells (average ± SD for three independent experiments, performed in duplicate). EV, expression vector; hACE2; human angiotensin-converting enzyme 2; S, spike protein; TMPRSS2, transmembrane serine protease 2.

D and *E*). Syncytia formation and evaluation of protein location by immunofluorescence were similar between all mutants and WT S (Fig. 5). Interestingly, cellular extensions containing the S protein were observed for the WT and each of the mutants (Fig. 5, *white arrows*) (61). Finally, luciferase reporter gene assays were performed. While most of the mutants displayed fusion levels similar to WT S, three mutants exhibited significant changes (Fig. 4*F*). D839Y and D839N displayed significantly reduced levels of fusion compared with WT ($p < 0.01$ and $p < 0.05$, respectively), and P1263L showed a significant increase in fusion compared with WT ($p < 0.05$). These changes in fusion are unlikely to be due to significant differences in cell surface protein expression or cleavage levels, although it is worth noting that D839Y and D839N demonstrated a lower percent cleavage than other mutations tested, though this decrease was not statistically significant. These data may suggest that residues near the internal fusion peptide, where D839 is located, and residues in the cytoplasmic tail, where P1263 is located, may play an important role in controlling the fusion cascade.

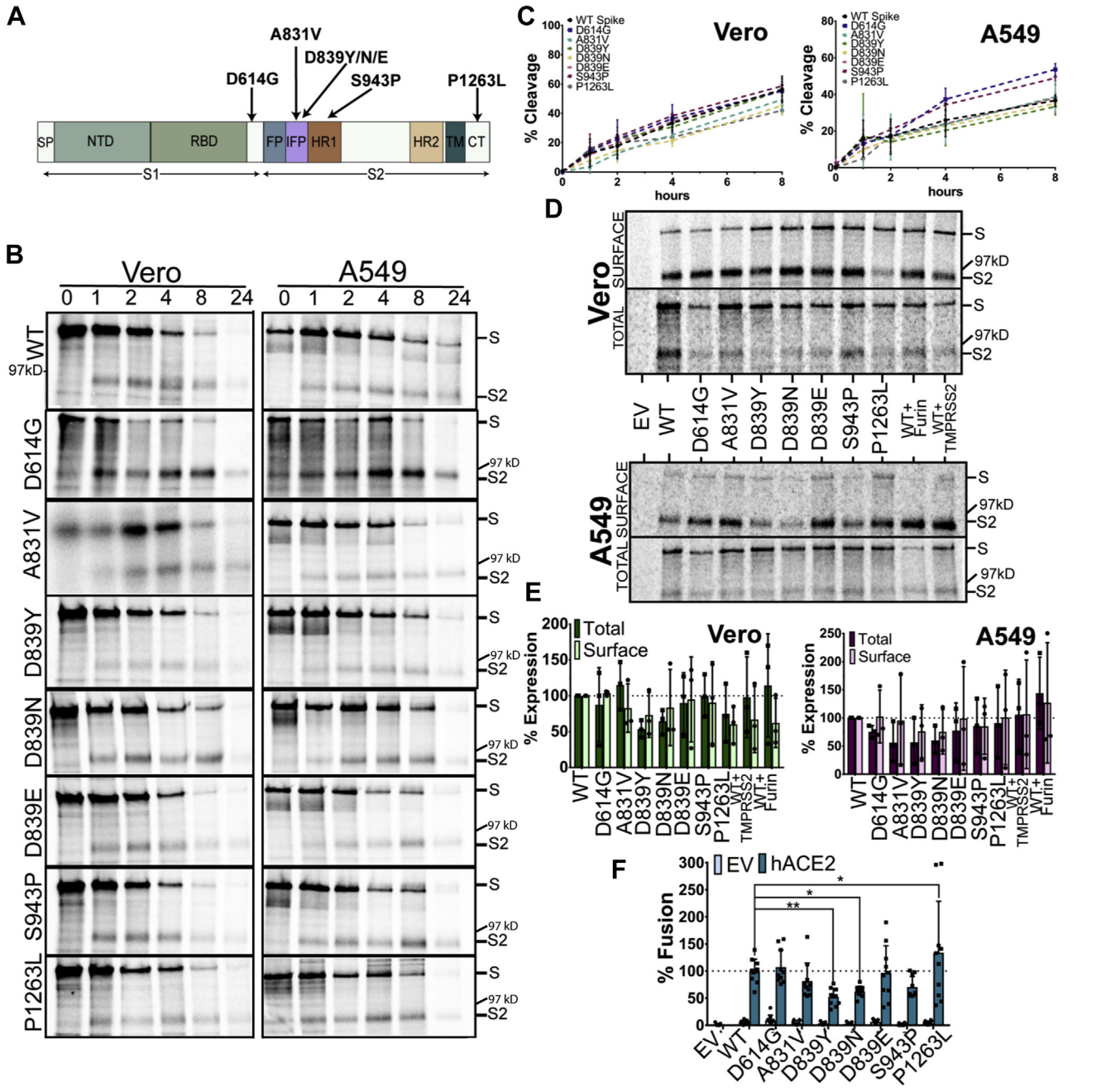

Figure 4. Spike S2 subunit mutations found in circulating variants variably affect spike-mediated cell–cell fusion. *A*, mutations in the S2 subunit of S identified in circulating SARS-CoV-2 variants. *B*, WT S or the mutants were transfected into Vero and A549 cells, metabolically labeled for 1 h, and chased for the times indicated. Percent cleavage was determined in (*C*) Vero and A549 cells (average ± SD for three independent experiments). *D*, surface biotinylation on cells expressing WT S or each mutant. *E*, total and surface protein expression normalized to WT S (average ± SD for three independent experiments). *F*, a luciferase reporter gene assay was performed using target cells expressing EV or hACE2, overlaid onto effector cells transfected with WT S or each mutant. Results are normalized to samples with WT S in the effector cells and hACE2 in target cells (average ± SD for three independent experiments, performed in duplicate). Significance was determined by two-way ANOVA: $*p < 0.05$ and $**p < 0.01$. EV, expression vector; hACE2, human angiotensin-converting enzyme 2; S, spike protein; SARS-CoV-2, severe acute respiratory syndrome coronavirus 2.

Trypsin accessibility and protein–protein association in select spike mutants

Since all the S cleavage site mutants exhibited defects in cleavage at the S1/S2 border, we evaluated the accessibility of this site using a trypsin treatment assay to determine if the lack of cleavage was due to misfolding in the S1/S2 border region. Vero or A549 cells were transfected with WT S or each cleavage mutant and metabolically labeled. Cell surface proteins were biotinylated, and then cells were either left untreated or treated with 0.3 μg/μl of TPCK–trypsin prior to lysis. When treated with exogenous TPCK–trypsin, both the del. PRRA and S1/S2 PRRAA mutants were efficiently cleaved at the S1/S2 border, shown by the appearance of a band corresponding to S2 in the lanes treated with trypsin (Fig. 6*A*, quantified in Fig. 6*B*). This suggests that the observed defects in cleavage at the S1/S2 border are not because of

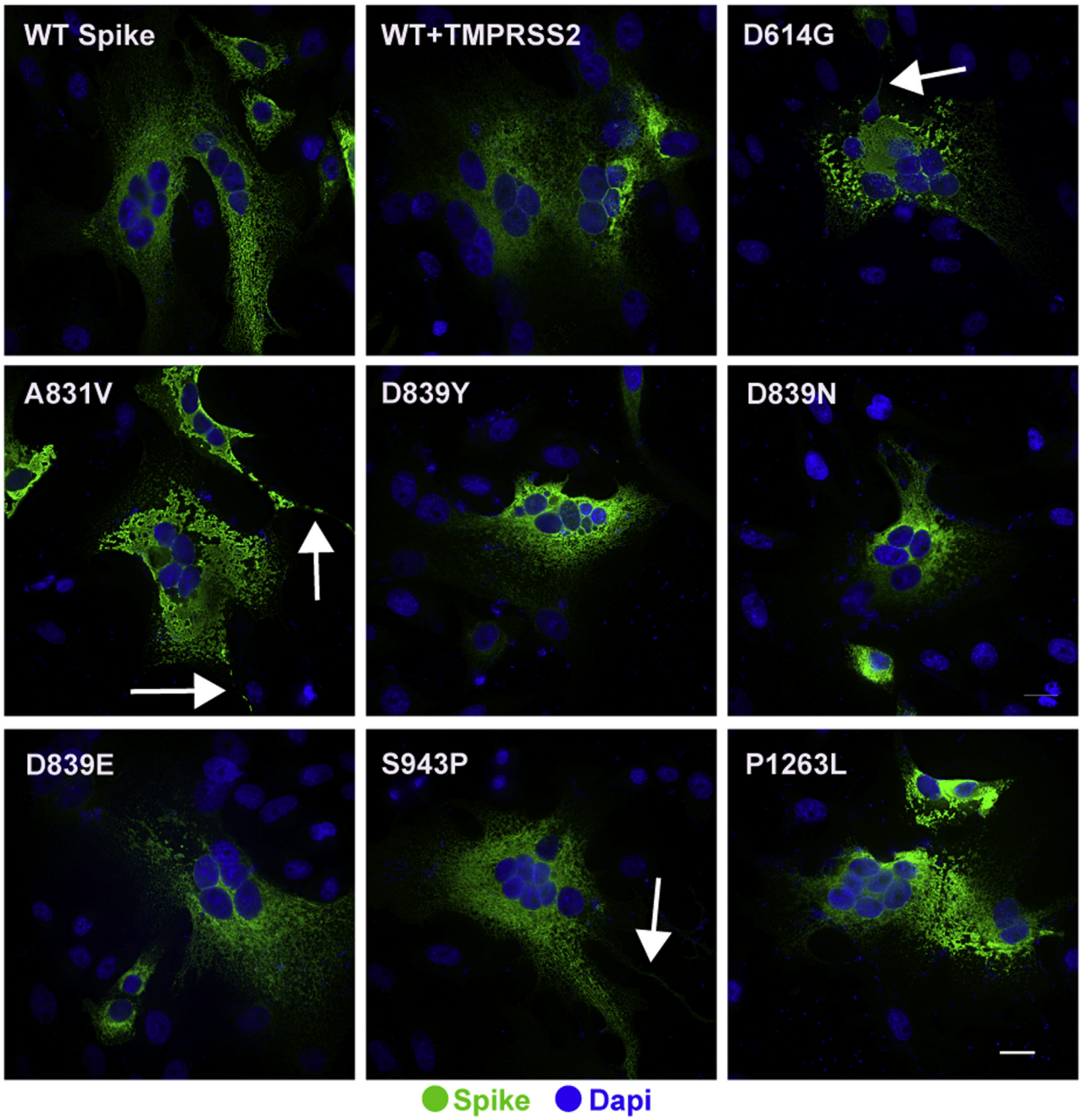

Figure 5. All circulating mutants form large syncytia, similar to WT spike. Immunofluorescence of WT S or the circulating mutants (S stained in *green*) transiently expressed in Vero cells. *White arrows* indicated S-positive cellular extensions. The magnification bar is 20 μM. S, spike protein.

inaccessibility at the site but rather to the removal of the furin consensus sequence. Interestingly, mutations at the downstream cath L or S2' potential cleavage sites also render defects in protein cleavage at the S1/S2 border site. However, treatment with exogenous trypsin did not significantly affect the amount of cleavage observed, a result consistent with a change in conformation that renders the S1/S2 border cleavage site inaccessible.

CoV S proteins associate as homotrimers shortly after synthesis and remain in this trimeric form throughout the fusion cascade (11, 14). To determine if proteolytic processing affects the stability of S trimer association, Vero or A549 cells transfected with WT S or mutants D614G, S1/S2 AAAAA, S2' AA, or WT S plus additional furin were metabolically labeled. After lysis and immunoprecipitation, samples were then treated at 50 °C or 100 °C prior to separation on nonreducing SDS-PAGE. When WT S was incubated at 50 °C prior to separation, species that correspond to a full-length S monomer, dimer, and trimer were observed (Fig. 6*C*). Interestingly, species that fall in between sizes corresponding to a monomer, dimer, and trimer (Fig. 6*C*, *red* and *purple* *) were also observed. These intermediate species may be the result of dimers or trimers made up of a mixture of full-length S protomers and cleaved S protomers. When WT S was incubated at

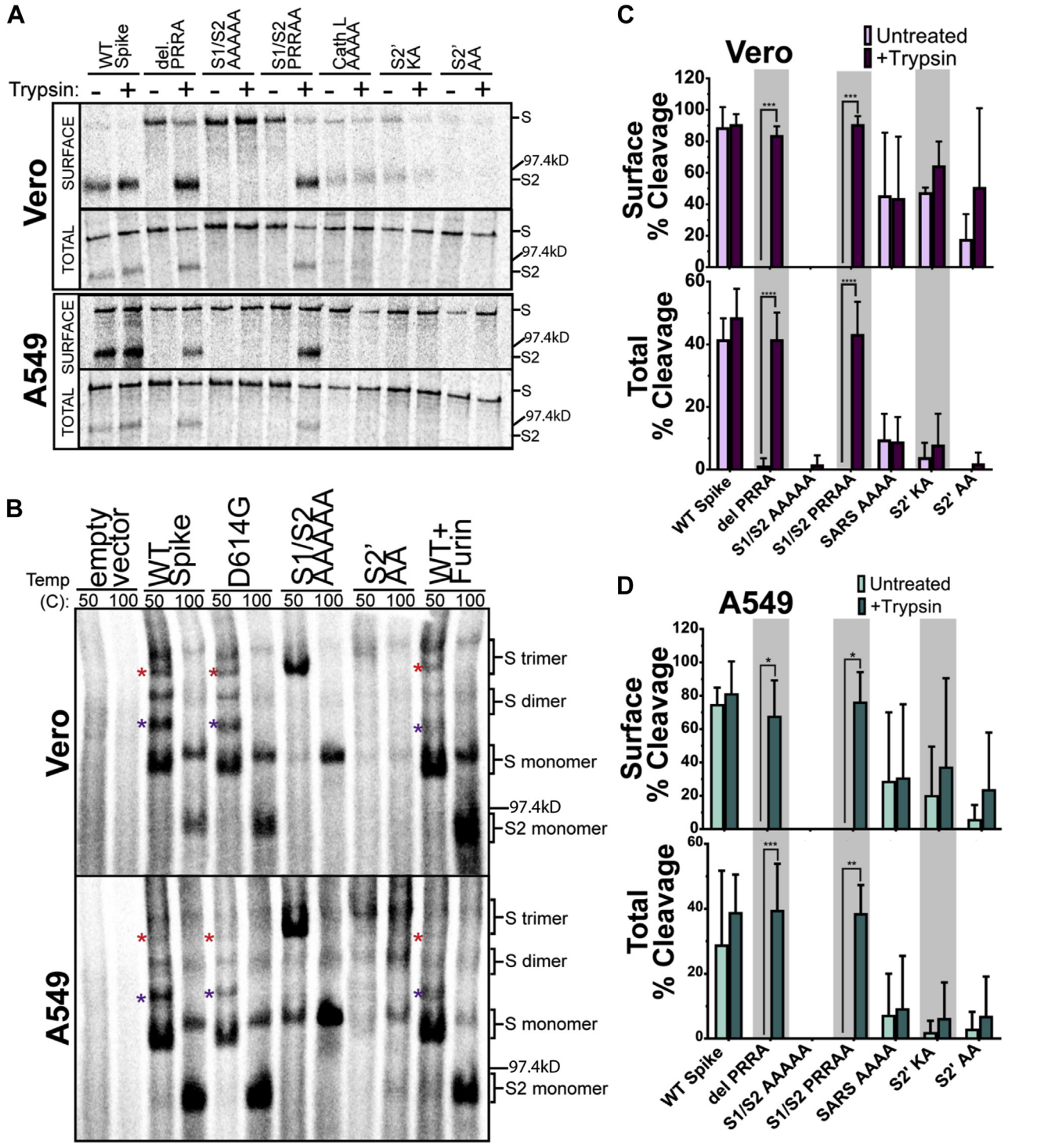

Figure 6. Mutations at downstream potential cleavage sites render the S1/S2 border cleavage site less accessible to proteases. *A*, Vero or A549 cells expressing WT S or S cleavage mutants were metabolically labeled for 6 h. Surface proteins were biotinylated, and samples were either treated for 10 min with TPCK–trypsin or left as untreated controls (as indicated). *B*, Vero or A549 cells expressing indicated proteins were metabolically labeled for 6 h. Samples were treated at the indicated temperatures before separation on a nonreducing SDS-PAGE. Oligomers are labeled on the right based on size, and colored * represents potential intermediate species (n = 3). Using band densitometry to quantify the bands in (*A*), percent cleavage was measured in (*C*) Vero and (*D*) A549 cells for both the surface (*top graphs*) and total (*bottom graphs*) populations (average ± SD for three independent experiments). Significance was determined by two-way ANOVA: *$p < 0.05$, **$p < 0.01$, ***$p < 0.0005$, and ****$p < 0.0001$. S, spike protein.

100 °C prior to separation, bands corresponding only to full-length S monomer, dimer, trimers, and cleaved S2 monomers were apparent. Similar results were also observed in D614G samples, suggesting that species containing cleaved protomers may be less stable. Consistent with these data, the S1/S2 AAAAA mutant, which cannot undergo cleavage at the S1/S2 border site, migrated primarily as a trimeric species after 50 °C incubation, with little monomer or dimer observed. In

addition, when WT S was coexpressed with furin (shown to increase S cleavage in Fig. 1, *E* and *F*), the predominant observed species was monomeric, after both 50 °C and 100 °C incubation. Overall, these results suggest that cleavage at the S1/S2 border alters the stability of S trimeric association.

Furin or furin-like proteases in bat cells can cleave the S1/S2 border of SARS-CoV-2 spike

R. affinis horseshoe bats have been identified as the likely reservoir species for the novel SARS-CoV-2 (24). To understand the proteolytic processing, expression, and stability of CoV-2 S in a cell line closely related to its reservoir host, we utilized *Pteropus alecto* fetus (pt. fetus) or lung (pt. lung) cells (62) that have a furin enzyme with ∼90% sequence homology to bats in the Rhinolopus family. Our previous studies on paramyxovirus fusion protein cleavage have shown that efficient furin and cathepsin cleavage occurs in these cells, although the furin cleavage occurs with delayed kinetics compared with Vero or A549 cells (63).

Surface biotinylation demonstrated that WT S and the del. PRRA mutant were readily expressed at the surface at similar levels in both cell lines, with cleavage at the S1/S2 border only observed for WT S and not for the del. PRRA mutant (Fig. 7, *A* and *B*). Pulse-chase analysis showed that S expressed in both pt. lung and pt. fetus cells was cleaved at the S1/S2 border by 1 h, with cleavage extent reaching approximately 40% at 8 h and 60% at 24 h (Fig. 7, *C* and *D*). Thus, furin or other proteases in *P. alecto* cells are able to process S, although this processing occurred more slowly than in other mammalian cell lines (compare to Fig. 1*B*). Interestingly, some cleavage was also observed in both pt. lung and pt. fetus cells for the del. PRRA mutation (Fig. 7, *C* and *D*). In addition, the WT S and del. PRRA mutant were slightly less stable in the *P. alecto* cells, demonstrating about 30 to 50% protein remaining at 8 h and about 20% at 24 h (Fig. 7*E*). In contrast, previously used mammalian cell lines showed 60 to 90% of WT S remained at 8 h, with 30 to 50% at 24 h of chase (Fig. 1*C*).

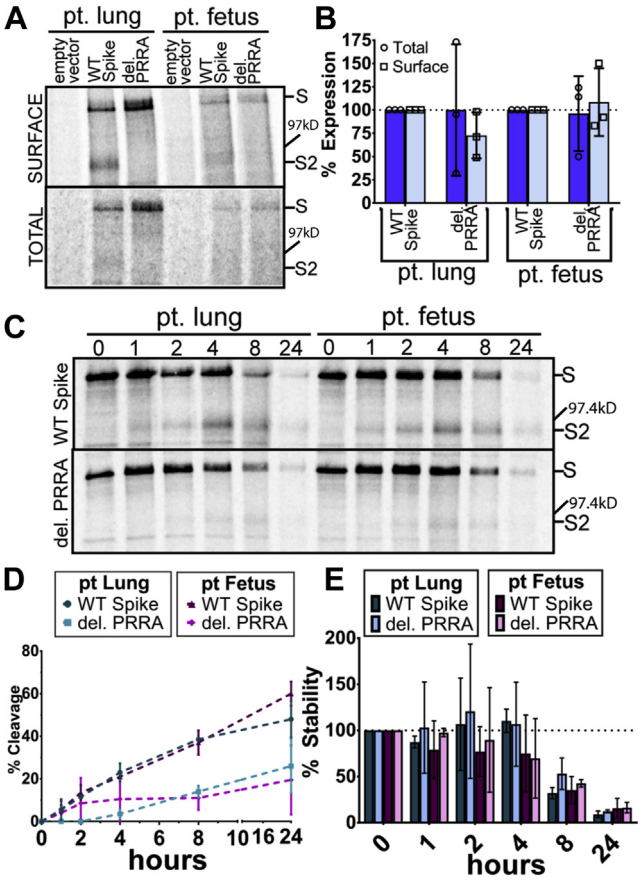

Figure 7. Furin or furin-like proteases in pteropus bat cells can cleave the S1/S2 border site of SARS-CoV-2 spike. *A*, surface biotinylation was performed on pteropus lung and pteropus fetus cells transfected with plasmids for WT S or the del. PRRA mutant. *B*, surface or total protein expression levels were quantified using band densitometry and normalized to WT S levels. *C*, pt. lung and pt. fetus cells were transfected with WT S or del. PRRA mutant, metabolically labeled for 1 h, and chased for the times indicated. Using band densitometry to quantify the bands in (*C*), results are expressed as (*D*) protein cleavage and (*E*) protein stability over the times indicated. (*B–E* average ± SD for three independent experiments). SARS-CoV-2, severe acute respiratory syndrome coronavirus 2.

Discussion

In this study, we present a detailed characterization of the cleavage patterns, protein stability, and cell–cell fusion function of the SARS-CoV-2 S protein, as well as analysis of mutations within the S2 subunit that may affect these important protein properties. Consistent with recently published work (25, 34, 46, 49, 50, 64), our analysis confirms that S is readily cleaved at the S1/S2 border in a variety of mammalian cell lines. In addition, we show for the first time that cleavage occurs in a bat cell line similar to the SARS-CoV-2 reservoir species. While cleavage appears to be primarily carried about by the cellular protease furin, the sequence at this border does have the ability to be cleaved by other members of the proprotein convertase family when furin is not present (46), and this likely accounts for the small amount of cleavage we observed in furin-negative LoVo cells.

In addition, we carefully assessed the role different proteases play in cell–cell fusion, finding that furin increases cell–cell fusion when present in the same cell as S, and TMPRSS2 increases cell–cell fusion when present in a target cell, consistent with previous studies (36, 45). Interestingly, when cell–cell fusion assays were performed using A549 cells as the effector cell (Fig. 2*C*), high background fusion levels were observed. This could be due to high endogenous levels of TMPRSS2 in this cell line compared with Vero cells, which were ultimately used for this experiment (Fig. S2*C*). High TMPRSS2 expression or exogenous treatment with trypsin has been shown to restore cell–cell fusion in low ACE2 receptor expression environments for SARS-CoV S (65, 66). It is also worth noting that coexpressing TMPRSS2 and hACE2 in the target cells (BSR/T7) leads to a double banding pattern for hACE2, suggesting that TMPRSS2 may be cleaving hACE2 (Fig. S2*C* (39)). Therefore, we cannot exclude the possibility that the increase in fusion observed when TMPRSS2 is present in these cells is due to an effect on hACE2. In addition to the effect of proteases on cell–cell fusion, we also assessed the effect of neuropilin-1, which has been suggested to be a

coreceptor for SARS-CoV-2 viral entry and may be key for SARS-CoV-2 infiltration of the neuronal network (51–53). We show that the presence of neuropilin-1 with hACE2 in target cells does not impact S-mediated cell–cell fusion (Fig. 2*E*). In addition, coexpressing neuropilin-1 with S in effector cells did not have an inhibitory effect on cell–cell fusion. While reports suggest that neuropilin-1 plays a role in viral entry of SARS-CoV-2, this indicates it does not play a significant role in S cell–cell fusion in our assay, although this was not investigated in neuronal cells.

The viral entry and cell–cell fusion pathways of SARS-CoV, Middle East respiratory syndrome (MERS)-CoV, and SARS-CoV-2 have several noteworthy commonalities but do have marked differences. They all share the ability to facilitate entry through endosomal pathways, with S proteolytic activation mediated by endosomal/lysosomal proteases (9, 18, 34, 36–38, 67–70). In addition, they all can utilize cell surface (such as TMPRSS2) or extracellular proteases (trypsin) for S activation and subsequent viral entry (9, 36, 37, 46, 65, 70–76). SARS-CoV-2 and MERS-CoV S differ from SARS-CoV S in that their S1/S2 border harbors a canonical furin cleavage motif (25, 26, 31), resulting in S preactivation by furin during synthesis and cellular trafficking, prior to reaching the cell surface or being incorporated into viral particles (18, 34, 36, 38, 73). This preactivation by furin likely enhances the ability of SARS-CoV-2 and MERS-CoV S to participate in cell–cell–mediated fusion without overexpression of cell surface or extracellular proteases (36, 45). Addition of this cleavage sequence in SARS-CoV S allows SARS-S to facilitate cell–cell fusion without exogenous proteases (36, 77). We show an increase in both syncytia formation and luciferase reporter gene assay fusion when cleavage at the S1/S2 border is enhanced by overexpression of furin (Fig. 2, *B* and *C*), confirming that furin cleavage of SARS-CoV-2 S plays a critical role in cell–cell fusion. Interestingly, furin cleavage is not required for SARS-CoV-2 infection (9, 34, 36, 46), although removal of the site or inhibition of furin does appear to attenuate the virus (34, 38, 46) and reduce cellular tropism (45).

The presence of a furin consensus sequence is not only a marked difference between SARS-CoV and SARS-CoV-2 but also one of the differences between SARS-CoV-2 and a similar CoV circulating in a bat population (24). Analysis of SARS-CoV-2 WT S in *P. alecto* cells demonstrates that this motif can be recognized and cleaved by furin in these cells (Fig. 7, *C* and *D*), although the kinetics of this cleavage are noticeably slower than in other mammalian cell lines (compare to Fig. 1*B*). Previous work has shown that the fusion proteins of Hendra virus, processed by cathepsins, and parainfluenza virus 5, processed by furin, are also cleaved in *P. alecto* cells (63). Pulse-chase analysis in this prior study demonstrated an increase in processing kinetics, although this kinetic difference can be accounted for by differences in protease expression levels between different bat cell lines (pt. kidney cells (63) and pt. lung and pt. fetus cells in our work), suggesting there may be cellular differences in protein trafficking or furin activity. Intriguingly, a CoV-2 S mutant with a deletion of the inserted PRRA residues still demonstrated some cleavage in both utilized bat cell lines (Fig. 7, *C* and *D*), while not showing any in Vero or A549 cells (Fig. 3, *C* and *D*). Earlier work on MERS-CoV S showed that furin or other proprotein convertases in bat cells can process MERS S S1/S2 border without the presence of a canonical recognition motif (78). Taken together, these results suggest that mutations in circulating bat CoVs that allow for human protease recognition at critical cleavage sites may be an important factor for zoonotic transmission of several CoVs.

Two other potential cleavage sites have been identified in work with other CoVs. The S2' site is essential for both SARS and MERS infection (11, 31, 79–81), whereas a cath L–activated site plays a critical role for SARS-CoV S (12, 19, 82, 83). Interestingly, mutations made at the S2' site of SARS-CoV-2 S significantly reduce S1/S2 border cleavage, both in our study and others (Fig. 3, *B–D* (45, 84)), even though the sites are distal from each other. A similar reduction in cleavage is observed when the conserved cathepsin site is mutated (Fig. 3, *B–D*). Our analysis of the published structures (2, 3, 85, 86) indicates that a full alanine mutation of this site may simply collapse the exposed S1/S2 loop. Our finding that exogenous trypsin treatment of cells expressing the S2' or cathepsin site mutants does not restore cleavage at the S1/S2 border (Fig. 5, *A* and *B*) suggests that these mutations result in proteins with altered furin loop structure (85), rendering it inaccessible. However, these mutants are still synthesized and trafficked to the surface despite not being cleaved (Fig. 3, *E–G*), thus this change in conformation is unlikely to have drastically misfolded the protein. These results suggest that there may be a dynamic interaction between the S1/S2 border and S2' cleavage sites in SARS-CoV-2 S needed to facilitate viral entry and cell–cell fusion. This dynamic control could also be regulated by S receptor binding exposing cryptic protease sites, although studies analyzing this in SARS and MERS S conflict on this topic (18, 68, 75, 87, 88).

We also assessed the effect on protein stability, cleavage, and cell–cell fusion function of a series of mutations in other regions of S. The D614G mutation emerged during 2020 and is now found in most circulating variants globally (47). D614G has been shown to increase S incorporation into viral particles (89), increase receptor binding (90, 91), and reduce S1 subunit shedding and particle infectivity (92). Importantly, the D614G mutant shifts S to favor a "heads up" conformation of the receptor-binding domain (91, 93, 94). In our study, the D614G mutation did not impact the cell–cell fusion function (Fig. 4*F*), expression, or stability of the protein (Fig. 4, *D* and *E* and Fig. S1), consistent with one previous study (84). Our fusion results however conflict with two previous studies that demonstrated that D614G increases cell–cell fusion, measured by cell depletion in flow cytometry (90), and syncytia formation in 293T and HeLa cells stably expressing hACE2 (95). These discrepancies may be due to differences in experimental conditions or cell types utilized. We are, however, the first to date to utilize a luciferase reporter gene assay to quantitate cell–cell fusion of a D614G S mutant. Using this assay, we also show that mutations found at two other residues (discovered in small and nondominant population subsets (48)) alter the

cell–cell fusion activity of S (Fig. 4*F*) without changing the overall protein expression or stability levels (Fig. 4, *D* and *E* and Fig. S1*D*). Mutations at D839, a residue within the internal fusion peptide, to the polar amino acids, tyrosine or asparagine, significantly reduce fusion. Interestingly, a mutation at this residue that conserves the negative charge, D839E, has no effect on fusion activity. The negative charge at this residue may play a role in the regulation of S-mediated fusion because of its location in the internal fusion peptide. Alternatively, this residue is in close proximity to C840, which may participate in a disulfide bond, so mutations at D839 may disrupt this disulfide bond, destabilizing the protein and changing fusion activity. In addition, mutation of residue P1263 to a leucine significantly increases S-mediated cell–cell fusion, suggesting that residues in the cytoplasmic tail may play a role in the S-promoted cell–cell fusion process. Notably, a study that removed the entire S cytoplasmic tail still observed syncytia formation at levels similar to WT S (84), indicating that regulation by the cytoplasmic tail may be complex or that the role of the cytoplasmic tail in fusion is not regulation but interaction with cellular host factors (96).

In this work, we also provide critical insight into the kinetics of protein cleavage and overall stability of CoV-2 S. S protein processing at the S1/S2 border occurs within 2 h of synthesis (Fig. 1, *A* and *B*; 1 h of label, 1 h of chase) in several mammalian cell lines (Vero, MEF, and A549) and continues to increase over time, reaching 60 to 80% protein cleavage by 8 h of chase time, depending on the cell type. Overexpression of furin increased the efficiency of S1/S2 border cleavage (Fig. 1, *D*–*F*), and this increase in cleavage may account for the increase in cell–cell fusion observed when furin is coexpressed with S (Fig. 2, *A*–*C* (36, 45)). In addition, we show edthat transiently transfected S is stable in several mammalian cells for 4 to 5 h postprotein synthesis with demonstrable turnover after this point (Fig. 1*C* and Fig. S1). This protein turnover is similar to turnover rates seen in PIV5 fusion protein, also activated by cellular furin (97), and slightly slower turnover than Hendra fusion protein, activated by cellular cathepsins (98, 99). Overexpression of cellular proteases that may process S did not affect these protein turnover rates. Interestingly, analysis of S in nonreducing conditions found that cleavage of the S1/S2 border appears to destabilize trimeric interactions (Fig. 6*B*). In these nonreducing conditions, no differences were observed in oligomeric stability between WT S and the D614G S mutations, despite the D614G favoring a "heads up" conformation (91, 93, 94) and Vero cells having sufficient levels of endogenous ACE2 to facilitate syncytia formation (Fig. S2*C*), suggesting that changes in receptor binding do not alter overall protein trimeric association. Notably, in these nonreducing conditions after a 50 °C treatment for WT S, the D614G mutant, and WT S + furin, bands between monomer, dimer, and trimer species are observed (Fig. 6*B*, indicated with an *). These intermediate species are not observed after treatment at 100 °C. These may represent protein oligomers that are not identically cleaved and are therefore partially destabilized, a phenomenon proposed for MERS-CoV S (31) and murine hepatitis virus CoV S, (100). Protein oligomers with differential proteolytic processing may also account for the small population of uncleaved protein we observed at the cell surface in our experiments (Figs. 3*E*, 4*D*, 6*A*, and 7*A*).

Through biochemical and cell biological analysis of the SARS-CoV-2 S protein, we have provided important observations about the stability, proteolytic processing, and requirements for cell–cell fusion of this highly sought-after therapeutic target. This information may be helpful in directing treatments that inhibit S protein fusion or for discerning methods to stabilize CoV-2 S in therapeutic development. Additional studies are needed to understand the potential interplay between S cleavage sites and how that may contribute to S protein function, as well as to further investigate spike S2 subunit regions that are critical for protein function.

Experimental procedures

Cell lines and culture

Vero cells (American Type Culture Collection), BSR T7/5 cells (provided by Karl-Klaus Conzelmann; Pettenkofer Institut), MEFs from cath L knockout mice (cath L-MEFs) (a gift from Terence Dermody; University of Pittsburgh), and *P. alecto* bat cells harvested from fetus (pt. fetus) and lung (pt. lung) (a gift from Linfa Wang; Duke-NUS) (62) were all maintained in Dulbecco's modified Eagle's medium (DMEM; GE Healthcare), with 10% fetal bovine serum (FBS) and 1% penicillin/streptomycin. Every third passage, 0.5 mg/ml of G-418 (Invitrogen) was added to the culture media of BSR T7/5 cells to select for the expression of the T7 polymerase. A549 and human colon carcinoma LoVo cells (both purchased from American Type Culture Collection) were cultured in F12 Kaighn's Modification media (GE Healthcare) with 10% FBS and 1% penicillin/streptomycin.

Plasmids, antibodies, and mutagenesis

pCAGGS-SARS-CoV-2 spike was obtained from BEI Resources. pcDNA3.1(+)-hACE2 and pcDNA3.1(+)-TMPRSS2 were provided by Gaya Amarasinghe (Washington University). Human neuropilin-1 was expressed with an exogenous PTPα signal sequence from the pLEXm vector (from Craig Vander Kooi; University of Kentucky). SARS-CoV-2 S was subcloned into pUC57, and all S mutants were created in pUC57 using the QuikChange site-directed mutagenesis kit (Strategene) with primers purchased from Eurofins. Constructs were then subcloned back into the pCAGGS EV. Other plasmids utilized include pSG5-cath L (from Terence Dermody; University of Pittsburgh), pCAGGS-furin (Promega), and T7 promoted-luciferase (Promega). Antibodies anti-SARS spike glycoprotein (ab252690), specific to the S2 subunit, and anti-hACE2 (ab15348) were purchased from Abcam, and anti-TMPRSS2 (H-4) was purchased from Santa Cruz Biotechnology, Inc.

Gel electrophoresis and Western blotting

Proteins were separated on a 10% SDS-PAGE. For Western blot analysis, proteins were transferred to a polyvinylidene

difluoride membrane (Fisher Scientific) at 60 V for 100 min. After blocking with 5% milk in Tris-buffered saline + Tween-20 (TTBS) for 1 h, membranes were incubated with respective antibodies (anti-SARS S, 1:5000 dilution; anti-TMPRSS2, 1:1000 dilution; and anti-hACE2, 1:1000 dilution) at 4 °C overnight. Membranes were then washed with TTBS and incubated with (Li-Cor) secondary antibodies at 1:10,000 dilution in 5% milk solution for 1 h. Membranes were washed again with TTBS and deionized H_2O, before being imaged on the Odyssey Image Analyzer (Li-Cor).

Syncytia assay

Cells (Vero or A549) in 6-well plates were transiently transfected with 2 μg of either wt or mutant SARS-CoV-2 S protein plasmid with Lipofectamine 3000 (Invitrogen) at a ratio of 1:2:2 DNA:P3000:Lipofectamine 3000. For experiments with the addition of proteases, the total DNA transfected was kept constant at 2 μg; in those cases, we used 1 μg of S and 1 μg of the indicated protease. Syncytia formation was imaged at 24 and 48 hpt on a Nikon Ti2 at 20× magnification.

Luciferase reporter gene assay

Effector cells (Vero or A549) were plated in 12-well plates at 70 to 90% confluency and transfected with 1 μg of total DNA (0.4 μg of a T7 promoted luciferase plasmid, 0.6 μg of WT or mutant S protein or S protein with additional proteases). At the same time, BSR cells (constitutively expressing a T7 promoter) seeded in 6-well plates were transfected with 2 μg either empty pCAGGS or pcDNA3.1(+)-hACE2. At about 18 to 24 hpt, BSR cells were lifted using trypsin, centrifuged for 5 min at 1500 rpm, resuspended in normal DMEM + 10% FBS, and overlaid onto the S-expressing cells at a ratio of 1:1. Overlaid samples were then incubated at 37 °C for 9 h (or as described in the article). Samples were lysed in 100 μl of Reporter Gene Lysis buffer (Promega) and frozen overnight. Plates were then scraped on ice, lysates were vortexed for 10 s, centrifuged at 13,000 rpm for 1 min at 4 °C, and 20 μl of the supernatant was added to an opaque 96-well plate. Luciferase activity was measured on a SpectraMax iD3 (Molecular Devices) using a Luciferase Assay System (Promega). Background values were subtracted (empty pCAGGS in BSRs and effector cells), and luciferase activity was expressed as a percentage of WT S (effector cells) and hACE2 (BSR cells).

Surface biotinylation

Two micrograms of WT or mutant S protein was transfected into Vero or A549 cells using the Lipofectamine 3000 system (Invitrogen; ratios described previously). At about 18 to 24 hpt, cells were starved in Cys^-/Met^- media (Gibco) for 45 min and metabolically labeled for 6 h using 50 μCi of S^{35} (PerkinElmer) incorporated into Cys and Met (S^{35} Cys/Met). After the label, cells were washed once with PBS (pH 8) and incubated with 1 mg/ml of EZ-link Sulfo-NHS-biotin (Thermo Fisher) in PBS (pH 8) at 4 °C for 35 min and then at room temperature for 15 min. Next, the cells were lysed in 500 μl of radioimmunoprecipitation assay (RIPA) buffer (100 mM Tris–HCl [pH 7.4], 0.1% SDS, 1% Triton X-100, and 1% deoxycholic acid) containing 150 mM NaCl, protease inhibitors (1 U aprotinin, 1 mM PMSF [both from Sigma–Aldrich]), 5 mM iodoacetamide, and cOmplete EDTA-free Protease Inhibitor Cocktail Tablets (all from Sigma–Aldrich). Cell lysates were centrifuged at 55,000 rpm for 10 min, and the supernatant was incubated with anti-SARS S polyclonal antibody at 4 °C for 3 h. Following incubation, protein A conjugated to Sepharose beads (Cytiva) were added to the samples and incubated at 4 °C for an additional 30 min. Postincubation samples were washed two times with each RIPA buffer + 0.3 M NaCl, RIPA buffer + 0.15 M NaCl, and SDS-Wash II buffer (50 mM Tris–HCl [pH 7.4], 150 mM NaCl, and 2.5 mM EDTA). After buffer aspiration and addition of 10% SDS, samples were boiled for 10 min. The supernatant was removed to a separate tube. About 15 μl of supernatant was removed and added to an equal portion of 2× SDS-loading buffer and labeled "TOTAL." Biotinylation buffer (20 mM Tris [pH 8], 150 mM NaCl, 5 mM EDTA, 1% Triton X-100, and 0.2% bovine serum albumin) and streptavidin-conjugated beads were added to the remaining supernatant, and this was incubated at 4 °C for 1 h. Samples were again washed as described previously, and 2× SDS-loading buffer was added following the washes. Samples were boiled for 15 min and run on a 10% SDS-PAGE gel. Gels were dried and exposed on a phosphoscreen for 2 to 4 days, and then visualized using a Typhoon Imaging System (GE Healthcare). Bands were quantified using band densitometry using the ImageQuant software (GE Healthcare).

Time course immunoprecipitation

About 2 μg of WT or mutant S was transfected into Vero or A549 cells using the Lipofectamine 3000 system (ratios described previously). At about 18 to 24 hpt, cells were starved in Cys^-/Met^- media (Gibco) for 45 min and metabolically labeled for 1 h using 50 μCi of S^{35} Cys/Met. After the 1-h labeling, cells were washed once with PBS, and normal DMEM + 10% FBS was added for indicated times. Cells were then lysed in 500 μl of RIPA lysis buffer. Anti-SARS S polyclonal antibodies were used to immunoprecipitate the CoV-2 S protein as previously described, and the protein was analyzed on a 10% SDS-PAGE gel. Gels were dried and exposed on a phosphoscreen for 2 to 4 days and visualized using a Typhoon Imaging System. Bands were quantified using band densitometry using the ImageQuant software.

Nonreducing gel electrophoresis

Two micrograms of wt or mutant S was transfected into Vero or A549 cells using the Lipofectamine 3000 system (ratios described previously). At about 18 to 24 hpt, cells were starved in Cys^-/Met^- media (Gibco) for 45 min and metabolically labeled for 6 h using 50 μCi of S^{35} Cys/Met. Lysed cells were immunoprecipitated as described previously; however, after the washing steps, 30 μl of 2× SDS-loading buffer without DTT was added to each sample. Samples were treated at 50 °C or 100 °C, as indicated, for 20 min and analyzed on a

3.5% acrylamide gel under nonreducing conditions. The gel was dried, exposed, and imaged as described for surface biotinylation.

Immunofluorescence experiments

Subconfluent cells on coverslips in 6-well plates were transfected with 2 μg of DNA using the Lipofectamine 3000 transfection system (Invitrogen). At about 18 to 24 hpt, cells were fixed with 4% paraformaldehyde for 15 min at room temperature. Cells were permeabilized in a solution of 1% Triton X-100 in PBS + 0.02% sodium azide (PBSN) for 15 min at 4 °C. After permeabilization, coverslips were moved to a humidity chamber and blocked with 1% normal goat serum in PBSN for 1 h at 4 °C. Cells were labeled with anti-SARS S antibody (1:2000 dilution) in blocking buffer overnight at 4 °C or for 3 to 5 h at room temperature. Samples were washed with PBSN + 0.01% Tween-20 seven times and incubated for 1 h at 4 °C with goat anti-rabbit FITC (1:2000 dilution). Samples were again washed with PBSN + 0.01% Tween seven times and mounted onto slides using Vectashield mounting media (Vector Laboratories). Slides were imaged on an Axiovert 200M (Zeiss) at 63× magnification using Metamorph to collect Z-stacks and processed using Nikon NIS Elements.

Statistical analysis

Statistical analysis was performed using Prism 7 for Windows (GraphPad). A p value of <0.05 was considered statistically significant. Multiple comparison tests were generated using one-way or two-way ANOVA with Dunnett's multiple comparison test: $^{*}p < 0.05$, $^{**}p < 0.01$, $^{***}p < 0.0005$, and $^{****}p < 0.0001$.

Data availability

The datasets generated during and/or analyzed during the current study are available upon request from the corresponding author, Rebecca Dutch (rdutc2@uky.edu), on reasonable request.

Supporting information—This article contains supporting information.

Acknowledgments—We thank Craig Vander Kooi (University of Kentucky) for providing the neuropilin-1 expression plasmid and for providing structural insight. We also thank Gaya K. Amarasinghe (Washington University School of Medicine) for providing the TMPRSS2 and hACE2 expression plasmids and providing feedback regarding experimental design.

Author contributions—C. T. B., D. W. L., and R. E. D. conceptualization; C. T. B., H. E. N., R. T., J. M. B., K. B. B., and C.-Y. W. data curation; C. T. B., H. E. N., K. E., C. L. M., J. M. B., K. B. B., C.-Y. W., and R. E. D. formal analysis; C.T.B. and H. E. N. validation; C. T. B., H. E. N., K. E., and R. T. investigation; C. T. B., H. E. N., K. E., and C. L. M. visualization; C. T. B., C. L. M., C.-Y. W., and R. E. D. methodology; C. T. B. writing–original draft; C. T. B., H. E. N., K. E., C. L. M., R. T., J. M. B., K. B. B., D. W. L., and R. E. D. writing–review and editing; D. W. L. and R. E. D. resources; D. W. L. and R. E. D. project administration; R. E. D. supervision; R. E. D. funding acquisition.

Funding and additional information—Financial support was provided by the CCTS CURE Alliance pilot award from the University of Kentucky, National Institute of Allergy and Infectious Diseases, National Institutes of Health grant R01AI051517, and National Institutes of Health grant 2P20 RR02017 to R. E. D. The content is solely the responsibility of the authors and does not necessarily represent the official views of the National Institutes of Health.

Conflict of interest—The authors declare that they have no conflicts of interest with the contents of this article.

Abbreviations—The abbreviations used are: ACE2, angiotensin-converting enzyme 2; cath L, cathepsin L; CoV, coronavirus; COVID-19, coronavirus disease 2019; DMEM, Dulbecco's modified Eagle's medium; EV, expression vector; FBS, fetal bovine serum; hACE2, human ACE2; hpt, hours post transfection; MEF, mouse embryonic fibroblast; MERS, Middle East respiratory syndrome; PBSN, PBS + 0.02% sodium azide; RIPA, radioimmunoprecipitation assay; S, spike protein; SARS-CoV-2, severe acute respiratory syndrome coronavirus 2; TMPRSS2, transmembrane serine protease 2; TTBS, Tris-buffered saline + Tween-20.

References

1. Tortorici, M. A., and Veesler, D. (2019) Structural insights into coronavirus entry. *Adv. Virus Res.* **105**, 93–116
2. Walls, A. C., Park, Y. J., Tortorici, M. A., Wall, A., McGuire, A. T., and Veesler, D. (2020) Structure, function, and antigenicity of the SARS-CoV-2 spike glycoprotein. *Cell* **181**, 281–292.e6
3. Lan, J., Ge, J., Yu, J., Shan, S., Zhou, H., Fan, S., Zhang, Q., Shi, X., Wang, Q., Zhang, L., and Wang, X. (2020) Structure of the SARS-CoV-2 spike receptor-binding domain bound to the ACE2 receptor. *Nature* **581**, 215–220
4. Luan, J., Lu, Y., Jin, X., and Zhang, L. (2020) Spike protein recognition of mammalian ACE2 predicts the host range and an optimized ACE2 for SARS-CoV-2 infection. *Biochem. Biophys. Res. Commun.* **526**, 165–169
5. Wang, Q., Zhang, Y., Wu, L., Niu, S., Song, C., Zhang, Z., Lu, G., Qiao, C., Hu, Y., Yuen, K. Y., Wang, Q., Zhou, H., Yan, J., and Qi, J. (2020) Structural and functional basis of SARS-CoV-2 entry by using human ACE2. *Cell* **181**, 894–904.e9
6. Yan, R., Zhang, Y., Li, Y., Xia, L., Guo, Y., and Zhou, Q. (2020) Structural basis for the recognition of SARS-CoV-2 by full-length human ACE2. *Science* **367**, 1444–1448
7. Benton, D. J., Wrobel, A. G., Xu, P., Roustan, C., Martin, S. R., Rosenthal, P. B., Skehel, J. J., and Gamblin, S. J. (2020) Receptor binding and priming of the spike protein of SARS-CoV-2 for membrane fusion. *Nature* **588**, 327–330
8. Shang, J., Ye, G., Shi, K., Wan, Y., Luo, C., Aihara, H., Geng, Q., Auerbach, A., and Li, F. (2020) Structural basis of receptor recognition by SARS-CoV-2. *Nature* **581**, 221–224
9. Hoffmann, M., Kleine-Weber, H., Schroeder, S., Krüger, N., Herrler, T., Erichsen, S., Schiergens, T. S., Herrler, G., Wu, N. H., Nitsche, A., Müller, M. A., Drosten, C., and Pöhlmann, S. (2020) SARS-CoV-2 cell entry depends on ACE2 and TMPRSS2 and is blocked by a clinically proven protease inhibitor. *Cell* **181**, 271–280.e8
10. Zhou, P., Yang, X. L., Wang, X. G., Hu, B., Zhang, L., Zhang, W., Si, H. R., Zhu, Y., Li, B., Huang, C. L., Chen, H. D., Chen, J., Luo, Y., Guo, H., Jiang, R. D., *et al.* (2020) A pneumonia outbreak associated with a new coronavirus of probable bat origin. *Nature* **579**, 270–273
11. Millet, J. K., and Whittaker, G. R. (2018) Physiological and molecular triggers for SARS-CoV membrane fusion and entry into host cells. *Virology* **517**, 3–8

12. Millet, J. K., and Whittaker, G. R. (2015) Host cell proteases: Critical determinants of coronavirus tropism and pathogenesis. *Virus Res.* **202**, 120–134
13. Hulswit, R. J., de Haan, C. A., and Bosch, B. J. (2016) Coronavirus spike protein and tropism changes. *Adv. Virus Res.* **96**, 29–57
14. Harrison, S. C. (2015) Viral membrane fusion. *Virology* **479-480**, 498–507
15. Belouzard, S., Millet, J. K., Licitra, B. N., and Whittaker, G. R. (2012) Mechanisms of coronavirus cell entry mediated by the viral spike protein. *Viruses* **4**, 1011–1033
16. Gallagher, T. M., and Buchmeier, M. J. (2001) Coronavirus spike proteins in viral entry and pathogenesis. *Virology* **279**, 371–374
17. Shang, J., Wan, Y., Luo, C., Ye, G., Geng, Q., Auerbach, A., and Li, F. (2020) Cell entry mechanisms of SARS-CoV-2. *Proc. Natl. Acad. Sci. U. S. A.* **117**, 11727–11734
18. Li, F. (2016) Structure, function, and evolution of coronavirus spike proteins. *Annu. Rev. Virol.* **3**, 237–261
19. Matsuyama, S., Ujike, M., Morikawa, S., Tashiro, M., and Taguchi, F. (2005) Protease-mediated enhancement of severe acute respiratory syndrome coronavirus infection. *Proc. Natl. Acad. Sci. U. S. A.* **102**, 12543–12547
20. Zheng, Y., Shang, J., Yang, Y., Liu, C., Wan, Y., Geng, Q., Wang, M., Baric, R. S., and Li, F. (2018) Lysosomal proteases are a determinant of coronavirus tropism. *J. Virol.* **92**, e01504-18
21. Lu, G., Wang, Q., and Gao, G. F. (2015) Bat-to-human: Spike features determining 'host jump' of coronaviruses SARS-CoV, MERS-CoV, and beyond. *Trends Microbiol.* **23**, 468–478
22. Menachery, V. D., Dinnon, K. H., 3rd, Yount, B. L., Jr., McAnarney, E. T., Gralinkski, L. E., Hale, A., Graham, R. L., Scobey, T., Anthony, S. J., Wang, L., Graham, B., Randell, S. H., Lipkin, W. I., and Baric, R. S. (2020) Trypsin treatment unlocks barrier for zoonotic bat coronavirus infection. *J. Virol.* **94**, e01774-19
23. Zhou, H., Chen, X., Hu, T., Li, J., Song, H., Liu, Y., Wang, P., Liu, D., Yang, J., Holmes, E. C., Hughes, A. C., Bi, Y., and Shi, W. (2020) A novel bat coronavirus closely related to SARS-CoV-2 contains natural insertions at the S1/S2 cleavage site of the spike protein. *Curr. Biol.* **30**, 2196–2203.e3
24. Boni, M. F., Lemey, P., Jiang, X., Lam, T. T., Perry, B. W., Castoe, T. A., Rambaut, A., and Robertson, D. L. (2020) Evolutionary origins of the SARS-CoV-2 sarbecovirus lineage responsible for the COVID-19 pandemic. *Nat. Microbiol.* **5**, 1408–1417
25. Coutard, B., Valle, C., de Lamballerie, X., Canard, B., Seidah, N. G., and Decroly, E. (2020) The spike glycoprotein of the new coronavirus 2019-nCoV contains a furin-like cleavage site absent in CoV of the same clade. *Antiviral Res* **176**, 104742
26. Braun, E., and Sauter, D. (2019) Furin-mediated protein processing in infectious diseases and cancer. *Clin. Transl. Immunol.* **8**, e1073
27. Izaguirre, G. (2019) The proteolytic regulation of virus cell entry by furin and other proprotein convertases. *Viruses* **11**, 837
28. Seidah, N. G., and Prat, A. (2012) The biology and therapeutic targeting of the proprotein convertases. *Nat. Rev. Drug Discov.* **11**, 367–383
29. Chan, C. M., Woo, P. C., Lau, S. K., Tse, H., Chen, H. L., Li, F., Zheng, B. J., Chen, L., Huang, J. D., and Yuen, K. Y. (2008) Spike protein, S, of human coronavirus HKU1: Role in viral life cycle and application in antibody detection. *Exp. Biol. Med. (Maywood)* **233**, 1527–1536
30. Le Coupanec, A., Desforges, M., Meessen-Pinard, M., Dubé, M., Day, R., Seidah, N. G., and Talbot, P. J. (2015) Cleavage of a neuroinvasive human respiratory virus spike glycoprotein by proprotein convertases modulates neurovirulence and virus spread within the central nervous system. *PLoS Pathog.* **11**, e1005261
31. Millet, J. K., and Whittaker, G. R. (2014) Host cell entry of Middle East respiratory syndrome coronavirus after two-step, furin-mediated activation of the spike protein. *Proc. Natl. Acad. Sci. U. S. A.* **111**, 15214–15219
32. Claas, E. C., Osterhaus, A. D., van Beek, R., De Jong, J. C., Rimmelzwaan, G. F., Senne, D. A., Krauss, S., Shortridge, K. F., and Webster, R. G. (1998) Human influenza A H5N1 virus related to a highly pathogenic avian influenza virus. *Lancet* **351**, 472–477
33. Kido, H., Okumura, Y., Takahashi, E., Pan, H. Y., Wang, S., Yao, D., Yao, M., Chida, J., and Yano, M. (2012) Role of host cellular proteases in the pathogenesis of influenza and influenza-induced multiple organ failure. *Biochim. Biophys. Acta* **1824**, 186–194
34. [preprint] Johnson, B. A., Xie, X., Kalveram, B., Lokugamage, K. G., Muruato, A., Zou, J., Zhang, X., Juelich, T., Smith, J. K., Zhang, L., Bopp, N., Schindewolf, C., Vu, M., Vanderheiden, A., Swetnam, D., *et al.* (2020) Furin cleavage site is key to SARS-CoV-2 pathogenesis. *bioRxiv*. https://doi.org/10.1101/2020.08.26.268854
35. Sun, X., Tse, L. V., Ferguson, A. D., and Whittaker, G. R. (2010) Modifications to the hemagglutinin cleavage site control the virulence of a neurotropic H1N1 influenza virus. *J. Virol.* **84**, 8683–8690
36. Hoffmann, M., Kleine-Weber, H., and Pöhlmann, S. (2020) A multibasic cleavage site in the spike protein of SARS-CoV-2 is essential for infection of human lung cells. *Mol. Cell* **78**, 779–784.e5
37. [preprint] Ou, T., Mou, H., Zhang, L., Ojha, A., Choe, H., and Farzan, M. (2020) Hydroxychloroquine-mediated inhibition of SARS-CoV-2 entry is attenuated by TMPRSS2. *bioRxiv*. https://doi.org/10.1101/2020.07.22.216150
38. [preprint] Zhu, Y., Feng, F., Hu, G., Wang, Y., Yu, Y., Zhu, Y., Xu, W., Cai, X., Sun, Z., Han, W., Ye, R., Chen, H., Ding, Q., Cai, Q., Qu, D., *et al.* (2020) The S1/S2 boundary of SARS-CoV-2 spike protein modulates cell entry pathways and transmission. *bioRxiv*. https://doi.org/10.1101/2020.08.25.266775
39. Buchrieser, J., Dufloo, J., Hubert, M., Monel, B., Planas, D., Rajah, M. M., Planchais, C., Porrot, F., Guivel-Benhassine, F., Van der Werf, S., Casartelli, N., Mouquet, H., Bruel, T., and Schwartz, O. (2020) Syncytia formation by SARS-CoV-2-infected cells. *EMBO J.* **39**, e106267
40. Bussani, R., Schneider, E., Zentilin, L., Collesi, C., Ali, H., Braga, L., Volpe, M. C., Colliva, A., Zanconati, F., Berlot, G., Silvestri, F., Zacchigna, S., and Giacca, M. (2020) Persistence of viral RNA, pneumocyte syncytia and thrombosis are hallmarks of advanced COVID-19 pathology. *EBioMedicine* **61**, 103104
41. Stadlmann, S., Hein-Kuhnt, R., and Singer, G. (2020) Viropathic multinuclear syncytial giant cells in bronchial fluid from a patient with COVID-19. *J. Clin. Pathol.* **73**, 607–608
42. Oprinca, G. C., and Muja, L. A. (2020) Postmortem examination of three SARS-CoV-2-positive autopsies including histopathologic and immunohistochemical analysis. *Int. J. Legal Med.* **135**, 329–339
43. Tian, S., Hu, W., Niu, L., Liu, H., Xu, H., and Xiao, S. Y. (2020) Pulmonary pathology of early-phase 2019 novel coronavirus (COVID-19) pneumonia in two patients with lung cancer. *J. Thorac. Oncol.* **15**, 700–704
44. Xu, Z., Shi, L., Wang, Y., Zhang, J., Huang, L., Zhang, C., Liu, S., Zhao, P., Liu, H., Zhu, L., Tai, Y., Bai, C., Gao, T., Song, J., Xia, P., *et al.* (2020) Pathological findings of COVID-19 associated with acute respiratory distress syndrome. *Lancet Respir. Med.* **8**, 420–422
45. [preprint] Hörnich, B. F., Großkopf, A. K., Schlagowski, S., Tenbusch, M., Kleine-Weber, H., Neipel, F., Stahl-Hennig, C., and Hahn, A. S. (2020) SARS-CoV-2 and SARS-CoV spike-mediated cell-cell fusion differ in the requirements for receptor expression and proteolytic activation and are not inhibited by Bromhexine. *bioRxiv*. https://doi.org/10.1101/2020.07.25.221135
46. [preprint] Papa, G., Mallery, D. L., Albecka, A., Welch, L., Cattin-Ortolá, J., Luptak, J., Paul, D., McMahon, H. T., Goodfellow, I. G., Carter, A., Munro, S., and James, L. C. (2020) Furin cleavage of SARS-CoV-2 spike promotes but is not essential for infection and cell-cell fusion. *bioRxiv*. https://doi.org/10.1101/2020.08.13.243303
47. Korber, B., Fischer, W. M., Gnanakaran, S., Yoon, H., Theiler, J., Abfalterer, W., Hengartner, N., Giorgi, E. E., Bhattacharya, T., Foley, B., Hastie, K. M., Parker, M. D., Partridge, D. G., Evans, C. M., Freeman, T. M., *et al.* (2020) Tracking changes in SARS-CoV-2 spike: Evidence that D614G increases infectivity of the COVID-19 virus. *Cell* **182**, 812–827.e19
48. [preprint] Korber, B., Fischer, W., Gnanakaran, S., Yoon, H., Theiler, J., Abfalterer, W., Foley, B., Giorgi, E., Bhattacharya, T., Parker, M., Partridge, D., Evans, C., Freeman, T., de Silva, T., LaBranche, C., *et al.* (2020) Spike mutation pipeline reveals the emergence of a more

transmissible form of SARS-CoV-2. *bioRxiv*. https://doi.org/10.1101/2020.04.29.069054
49. Cheng, Y. W., Chao, T. L., Li, C. L., Chiu, M. F., Kao, H. C., Wang, S. H., Pang, Y. H., Lin, C. H., Tsai, Y. M., Lee, W. H., Tao, M. H., Ho, T. C., Wu, P. Y., Jang, L. T., Chen, P. J., *et al.* (2020) Furin inhibitors block SARS-CoV-2 spike protein cleavage to suppress virus production and cytopathic effects. *Cell Rep.* **33**, 108254
50. Li, W. (2020) Delving deep into the structural aspects of a furin cleavage site inserted into the spike protein of SARS-CoV-2: A structural biophysical perspective. *Biophys. Chem.* **264**, 106420
51. Cantuti-Castelvetri, L., Ojha, R., Pedro, L. D., Djannatian, M., Franz, J., Kuivanen, S., van der Meer, F., Kallio, K., Kaya, T., Anastasina, M., Smura, T., Levanov, L., Szirovicza, L., Tobi, A., Kallio-Kokko, H., *et al.* (2020) Neuropilin-1 facilitates SARS-CoV-2 cell entry and infectivity. *Science* **370**, 856–860
52. Daly, J. L., Simonetti, B., Klein, K., Chen, K. E., Williamson, M. K., Antón-Plágaro, C., Shoemark, D. K., Simón-Gracia, L., Bauer, M., Hollandi, R., Greber, U. F., Horvath, P., Sessions, R. B., Helenius, A., Hiscox, J. A., *et al.* (2020) Neuropilin-1 is a host factor for SARS-CoV-2 infection. *Science* **370**, 861–865
53. Davies, J., Randeva, H. S., Chatha, K., Hall, M., Spandidos, D. A., Karteris, E., and Kyrou, I. (2020) Neuropilin-1 as a new potential SARS-CoV-2 infection mediator implicated in the neurologic features and central nervous system involvement of COVID-19. *Mol. Med. Rep.* **22**, 4221–4226
54. Biswas, N. K., and Majumder, P. P. (2020) Analysis of RNA sequences of 3636 SARS-CoV-2 collected from 55 countries reveals selective sweep of one virus type. *Indian J. Med. Res.* **151**, 450–458
55. Gong, Y. N., Tsao, K. C., Hsiao, M. J., Huang, C. G., Huang, P. N., Huang, P. W., Lee, K. M., Liu, Y. C., Yang, S. L., Kuo, R. L., Chen, K. F., Liu, Y. C., Huang, S. Y., Huang, H. I., Liu, M. T., *et al.* (2020) SARS-CoV-2 genomic surveillance in Taiwan revealed novel ORF8-deletion mutant and clade possibly associated with infections in Middle East. *Emerg. Microbes Infect.* **9**, 1457–1466
56. Isabel, S., Graña-Miraglia, L., Gutierrez, J. M., Bundalovic-Torma, C., Groves, H. E., Isabel, M. R., Eshaghi, A., Patel, S. N., Gubbay, J. B., Poutanen, T., Guttman, D. S., and Poutanen, S. M. (2020) Evolutionary and structural analyses of SARS-CoV-2 D614G spike protein mutation now documented worldwide. *Sci. Rep.* **10**, 14031
57. Islam, O. K., Al-Emran, H. M., Hasan, M. S., Anwar, A., Jahid, M. I. K., and Hossain, M. A. (2020) Emergence of European and North American mutant variants of SARS-CoV-2 in South-East Asia. *Transbound. Emerg. Dis.* **68**, 824–832
58. Koyama, T., Platt, D., and Parida, L. (2020) Variant analysis of SARS-CoV-2 genomes. *Bull. World Health Organ.* **98**, 495–504
59. Koyama, T., Weeraratne, D., Snowdon, J. L., and Parida, L. (2020) Emergence of drift variants that may affect COVID-19 vaccine development and antibody treatment. *Pathogens* **9**, 324
60. Mercatelli, D., and Giorgi, F. M. (2020) Geographic and genomic distribution of SARS-CoV-2 mutations. *Front. Microbiol.* **11**, 1800
61. Caldas, L. A., Carneiro, F. A., Higa, L. M., Monteiro, F. L., da Silva, G. P., da Costa, L. J., Durigon, E. L., Tanuri, A., and de Souza, W. (2020) Ultrastructural analysis of SARS-CoV-2 interactions with the host cell via high resolution scanning electron microscopy. *Sci. Rep.* **10**, 16099
62. Crameri, G., Todd, S., Grimley, S., McEachern, J. A., Marsh, G. A., Smith, C., Tachedjian, M., De Jong, C., Virtue, E. R., Yu, M., Bulach, D., Liu, J. P., Michalski, W. P., Middleton, D., Field, H. E., *et al.* (2009) Establishment, immortalisation and characterisation of pteropid bat cell lines. *PLoS One* **4**, e8266
63. El Najjar, F., Lampe, L., Baker, M. L., Wang, L. F., and Dutch, R. E. (2015) Analysis of cathepsin and furin proteolytic enzymes involved in viral fusion protein activation in cells of the bat reservoir host. *PLoS One* **10**, e0115736
64. Örd, M., Faustova, I., and Loog, M. (2020) The sequence at spike S1/S2 site enables cleavage by furin and phospho-regulation in SARS-CoV2 but not in SARS-CoV1 or MERS-CoV. *Sci. Rep.* **10**, 16944
65. Glowacka, I., Bertram, S., Müller, M. A., Allen, P., Soilleux, E., Pfefferle, S., Steffen, I., Tsegaye, T. S., He, Y., Gnirss, K., Niemeyer, D., Schneider, H., Drosten, C., and Pöhlmann, S. (2011) Evidence that TMPRSS2 activates the severe acute respiratory syndrome coronavirus spike protein for membrane fusion and reduces viral control by the humoral immune response. *J. Virol.* **85**, 4122–4134
66. Simmons, G., Bertram, S., Glowacka, I., Steffen, I., Chaipan, C., Agudelo, J., Lu, K., Rennekamp, A. J., Hofmann, H., Bates, P., and Pöhlmann, S. (2011) Different host cell proteases activate the SARS-coronavirus spike-protein for cell-cell and virus-cell fusion. *Virology* **413**, 265–274
67. Huang, I. C., Bosch, B. J., Li, F., Li, W., Lee, K. H., Ghiran, S., Vasilieva, N., Dermody, T. S., Harrison, S. C., Dormitzer, P. R., Farzan, M., Rottier, P. J., and Choe, H. (2006) SARS coronavirus, but not human coronavirus NL63, utilizes cathepsin L to infect ACE2-expressing cells. *J. Biol. Chem.* **281**, 3198–3203
68. Simmons, G., Gosalia, D. N., Rennekamp, A. J., Reeves, J. D., Diamond, S. L., and Bates, P. (2005) Inhibitors of cathepsin L prevent severe acute respiratory syndrome coronavirus entry. *Proc. Natl. Acad. Sci. U. S. A.* **102**, 11876–11881
69. Simmons, G., Reeves, J. D., Rennekamp, A. J., Amberg, S. M., Piefer, A. J., and Bates, P. (2004) Characterization of severe acute respiratory syndrome-associated coronavirus (SARS-CoV) spike glycoprotein-mediated viral entry. *Proc. Natl. Acad. Sci. U. S. A.* **101**, 4240–4245
70. Qian, Z., Dominguez, S. R., and Holmes, K. V. (2013) Role of the spike glycoprotein of human Middle East respiratory syndrome coronavirus (MERS-CoV) in virus entry and syncytia formation. *PLoS One* **8**, e76469
71. Bertram, S., Glowacka, I., Müller, M. A., Lavender, H., Gnirss, K., Nehlmeier, I., Niemeyer, D., He, Y., Simmons, G., Drosten, C., Soilleux, E. J., Jahn, O., Steffen, I., and Pöhlmann, S. (2011) Cleavage and activation of the severe acute respiratory syndrome coronavirus spike protein by human airway trypsin-like protease. *J. Virol.* **85**, 13363–13372
72. Gierer, S., Bertram, S., Kaup, F., Wrensch, F., Heurich, A., Krämer-Kühl, A., Welsch, K., Winkler, M., Meyer, B., Drosten, C., Dittmer, U., von Hahn, T., Simmons, G., Hofmann, H., and Pöhlmann, S. (2013) The spike protein of the emerging betacoronavirus EMC uses a novel coronavirus receptor for entry, can be activated by TMPRSS2, and is targeted by neutralizing antibodies. *J. Virol.* **87**, 5502–5511
73. Gierer, S., Müller, M. A., Heurich, A., Ritz, D., Springstein, B. L., Karsten, C. B., Schendzielorz, A., Gnirß, K., Drosten, C., and Pöhlmann, S. (2015) Inhibition of proprotein convertases abrogates processing of the Middle Eastern respiratory syndrome coronavirus spike protein in infected cells but does not reduce viral infectivity. *J. Infect. Dis.* **211**, 889–897
74. Kam, Y. W., Okumura, Y., Kido, H., Ng, L. F., Bruzzone, R., and Altmeyer, R. (2009) Cleavage of the SARS coronavirus spike glycoprotein by airway proteases enhances virus entry into human bronchial epithelial cells in vitro. *PLoS One* **4**, e7870
75. Shirato, K., Kawase, M., and Matsuyama, S. (2013) Middle East respiratory syndrome coronavirus infection mediated by the transmembrane serine protease TMPRSS2. *J. Virol.* **87**, 12552–12561
76. Shulla, A., Heald-Sargent, T., Subramanya, G., Zhao, J., Perlman, S., and Gallagher, T. (2011) A transmembrane serine protease is linked to the severe acute respiratory syndrome coronavirus receptor and activates virus entry. *J. Virol.* **85**, 873–882
77. Follis, K. E., York, J., and Nunberg, J. H. (2006) Furin cleavage of the SARS coronavirus spike glycoprotein enhances cell-cell fusion but does not affect virion entry. *Virology* **350**, 358–369
78. Yang, Y., Liu, C., Du, L., Jiang, S., Shi, Z., Baric, R. S., and Li, F. (2015) Two mutations were critical for bat-to-human transmission of Middle East respiratory syndrome coronavirus. *J. Virol.* **89**, 9119–9123
79. Belouzard, S., Chu, V. C., and Whittaker, G. R. (2009) Activation of the SARS coronavirus spike protein via sequential proteolytic cleavage at two distinct sites. *Proc. Natl. Acad. Sci. U. S. A.* **106**, 5871–5876
80. Belouzard, S., Madu, I., and Whittaker, G. R. (2010) Elastase-mediated activation of the severe acute respiratory syndrome coronavirus spike protein at discrete sites within the S2 domain. *J. Biol. Chem.* **285**, 22758–22763

81. Heald-Sargent, T., and Gallagher, T. (2012) Ready, set, fuse! The coronavirus spike protein and acquisition of fusion competence. *Viruses* **4**, 557–580
82. Bosch, B. J., Bartelink, W., and Rottier, P. J. (2008) Cathepsin L functionally cleaves the severe acute respiratory syndrome coronavirus class I fusion protein upstream of rather than adjacent to the fusion peptide. *J. Virol.* **82**, 8887–8890
83. Matsuyama, S., Nagata, N., Shirato, K., Kawase, M., Takeda, M., and Taguchi, F. (2010) Efficient activation of the severe acute respiratory syndrome coronavirus spike protein by the transmembrane protease TMPRSS2. *J. Virol.* **84**, 12658–12664
84. [preprint] Nguyen, H. T., Zhang, S., Wang, Q., Anang, S., Wang, J., Ding, H., Kappes, J. C., and Sodroski, J. (2020) Spike glycoprotein and host cell determinants of SARS-CoV-2 entry and cytopathic effects. *bioRxiv*. https://doi.org/10.1101/2020.10.22.351569
85. Lemmin, T., Kalbermatter, D., Harder, D., Plattet, P., and Fotiadis, D. (2020) Structures and dynamics of the novel S1/S2 protease cleavage site loop of the SARS-CoV-2 spike glycoprotein. *J. Struct. Biol. X* **4**, 100038
86. Wrapp, D., Wang, N., Corbett, K. S., Goldsmith, J. A., Hsieh, C. L., Abiona, O., Graham, B. S., and McLellan, J. S. (2020) Cryo-EM structure of the 2019-nCoV spike in the prefusion conformation. *Science* **367**, 1260–1263
87. Beniac, D. R., deVarennes, S. L., Andonov, A., He, R., and Booth, T. F. (2007) Conformational reorganization of the SARS coronavirus spike following receptor binding: Implications for membrane fusion. *PLoS One* **2**, e1082
88. Li, F., Berardi, M., Li, W., Farzan, M., Dormitzer, P. R., and Harrison, S. C. (2006) Conformational states of the severe acute respiratory syndrome coronavirus spike protein ectodomain. *J. Virol.* **80**, 6794–6800
89. Zhang, L., Jackson, C. B., Mou, H., Ojha, A., Peng, H., Quinlan, B. D., Rangarajan, E. S., Pan, A., Vanderheiden, A., Suthar, M. S., Li, W., Izard, T., Rader, C., Farzan, M., and Choe, H. (2020) SARS-CoV-2 spike-protein D614G mutation increases virion spike density and infectivity. *Nat. Commun.* **11**, 6013
90. [preprint] Ogawa, J., Zhu, W., Tonnu, N., Singer, O., Hunter, T., Ryan, A. L., and Pao, G. M. (2020) The D614G mutation in the SARS-CoV2 spike protein increases infectivity in an ACE2 receptor dependent manner. *bioRxiv*. https://doi.org/10.1101/2020.07.21.214932
91. Yurkovetskiy, L., Wang, X., Pascal, K. E., Tomkins-Tinch, C., Nyalile, T. P., Wang, Y., Baum, A., Diehl, W. E., Dauphin, A., Carbone, C., Veinotte, K., Egri, S. B., Schaffner, S. F., Lemieux, J. E., Munro, J. B., *et al.* (2020) Structural and functional analysis of the D614G SARS-CoV-2 spike protein variant. *Cell* **183**, 739–751.e8
92. [preprint] Zhang, L., Jackson, C. B., Mou, H., Ojha, A., Rangarajan, E. S., Izard, T., Farzan, M., and Choe, H. (2020) The D614G mutation in the SARS-CoV-2 spike protein reduces S1 shedding and increases infectivity. *bioRxiv*. https://doi.org/10.1101/2020.06.12.148726
93. [preprint] Mansbach, R. A., Chakraborty, S., Nguyen, K., Montefiori, D. C., Korber, B., and Gnanakaran, S. (2020) The SARS-CoV-2 spike variant D614G favors an open conformational state. *bioRxiv*. https://doi.org/10.1101/2020.07.26.219741
94. [preprint] Plante, J. A., Liu, Y., Liu, J., Xia, H., Johnson, B. A., Lokugamage, K. G., Zhang, X., Muruato, A. E., Zou, J., Fontes-Garfias, C. R., Mirchandani, D., Scharton, D., Bilello, J. P., Ku, Z., An, Z., *et al.* (2020) Spike mutation D614G alters SARS-CoV-2 fitness and neutralization susceptibility. *bioRxiv*. https://doi.org/10.1101/2020.09.01.278689
95. Jiang, X., Zhang, Z., Wang, C., Ren, H., Gao, L., Peng, H., Niu, Z., Ren, H., Huang, H., and Sun, Q. (2020) Bimodular effects of D614G mutation on the spike glycoprotein of SARS-CoV-2 enhance protein processing, membrane fusion, and viral infectivity. *Signal Transduct. Target. Ther.* **5**, 268
96. Buonvino, S., and Melino, S. (2020) New consensus pattern in spike CoV-2: Potential implications in coagulation process and cell-cell fusion. *Cell Death Discov.* **6**, 134
97. Branttie, J. M., and Dutch, R. E. (2020) Parainfluenza virus 5 fusion protein maintains pre-fusion stability but not fusogenic activity following mutation of a transmembrane leucine/isoleucine domain. *J. Gen. Virol.* **101**, 467–472
98. Slaughter, K. B., and Dutch, R. E. (2019) Transmembrane domain dissociation is required for Hendra virus F protein fusogenic activity. *J. Virol.* **93**, e01069-19
99. Webb, S., Nagy, T., Moseley, H., Fried, M., and Dutch, R. (2017) Hendra virus fusion protein transmembrane domain contributes to pre-fusion protein stability. *J. Biol. Chem.* **292**, 5685–5694
100. Kawase, M., Kataoka, M., Shirato, K., and Matsuyama, S. (2019) Biochemical analysis of coronavirus spike glycoprotein conformational intermediates during membrane fusion. *J. Virol.* **93**